

1 **Exploring the Severe Winter Haze in Beijing: Impact of**
2 **Synoptic Weather, Regional Transport and Heterogeneous**
3 **Reactions**

4
5 **G. J. Zheng¹, F. K. Duan¹, H. Su², Y. L. Ma¹, Y. Cheng¹, B. Zheng¹, Q. Zhang^{3,6}, T.**
6 **Huang⁴, T. Kimoto⁴, D. Chang², U. Pöschl², Y. F. Cheng^{2,*}, and K. B. He^{1,5,6,*}**

7 [1] State Key Joint Laboratory of Environment Simulation and Pollution Control, School of
8 Environment, Tsinghua University, Beijing 100084, China

9 [2] Multiphase Chemistry Department, Max Planck Institute for Chemistry, D-55128, Mainz,
10 Germany

11 [3] Ministry of Education Key Laboratory for Earth System Modeling, Center for Earth
12 System Science, Tsinghua University, Beijing 100084, China

13 [4] Kimoto Electric Co., Ltd, 3-1 Funahashi-cho Tennoji-ku, Osaka 543-0024, Japan

14 [5] State Environmental Protection Key Laboratory of Sources and Control of Air Pollution
15 Complex, Beijing 100084, China

16 [6] Collaborative Innovation Center for Regional Environmental Quality, Beijing 100084,
17 China

18
19
20
21
22
23 Correspondence to: K. B. He (hekb@mail.tsinghua.edu.cn)

24 Y. F. Cheng (yafang.cheng@mpic.de)

26 **Abstract**

27 Extreme haze episodes repeatedly shrouded Beijing during the winter of 2012–2013, causing
28 major environmental and health problems. To better understand these extreme events, we
29 performed a model-assisted analysis of the hourly observation data of PM_{2.5} and its major
30 chemical compositions. The synthetic analysis shows that, (1) the severe winter haze was
31 driven by stable synoptic meteorological conditions over northeastern China, rather than by
32 an abrupt increase in anthropogenic emissions. (2) Secondary species, including organics,
33 sulfate, nitrate, and ammonium, were the major constituents of PM_{2.5} during this period. (3)
34 Due to the dimming effect of high loading of aerosol particles, gaseous oxidant concentrations
35 decreased significantly, suggesting a reduced production of secondary aerosols through gas
36 phase reactions. Surprisingly, the observational data reveals an enhanced production rate of
37 secondary aerosols, suggesting an important contribution from other formation pathways,
38 most likely heterogeneous reactions. These reactions appeared to be more efficient in
39 producing secondary inorganics aerosols than organic aerosols resulting in a strongly elevated
40 fraction of inorganics during heavily polluted periods. (4) Moreover, we found that high
41 aerosol concentration was a regional phenomenon. The accumulation process of aerosol
42 particles occurred successively from southeast cities to Beijing. The apparent sharp increase
43 in PM_{2.5} concentration of up to several hundred $\mu\text{g m}^{-3}$ per hour recorded in Beijing
44 represented rapid recovery from an interruption to the continuous pollution accumulation over
45 the region, rather than purely local chemical production. This suggests that regional transport
46 of pollutants played an important role during these severe pollution events.

47

48 **1 Introduction**

49 Severe haze episodes in the winter of 2012–2013 engulfed Beijing, as well as other cities in
50 southeastern China, causing one of the worst atmospheric pollution events in history. With
51 hourly fine particle ($\text{PM}_{2.5}$) concentrations up to $\sim 900 \mu\text{g}/\text{m}^3$, outdoor exposure caused
52 adverse health effects (Nel, 2005; Pöschl, 2005; Peplow, 2014), including severe respiratory
53 system related symptoms and deceases (Cao et al., 2014; Ouyang, 2013). Meanwhile the
54 visibility was reduced down to 100 m, which disrupted traffic with canceled flights and closed
55 highways. The government had to adopt emergency response measures to deal with these
56 pollution episodes (<http://english.sina.com/china/p/2013/0113/548263.html>). In addition to
57 massive amounts of primary particulate matter, high emissions in China provided plenty of
58 gas pollutants to serve as precursors for secondary aerosols (Zhang et al., 2009). Densely
59 distributed mega-cities (i.e., city clusters) have worsened this situation, contributing to
60 regional air pollution. Once the regional pollution is formed, the advection becomes less
61 effective in scavenging local pollutants (no clean air from upwind). Thus, the regional
62 pollution is more persistent compared with air pollution within a specific city. Moreover,
63 cities within this region could not eliminate their pollution solely by reducing local emissions
64 (Chan and Yao, 2008; Cheng et al. 2008a).

65 These extreme haze episodes attracted great scientific interest. The visibility impairment has
66 been attributed to scattering and absorption of solar radiation by aerosol particles (mostly
67 $\text{PM}_{2.5}$) and their hygroscopic growth under high relative humidity (Cheng et al., 2006; Cheng
68 et al., 2008b,c). Regional transport of pollutants was found to contribute considerably to
69 concentrations of $\text{PM}_{2.5}$ (Z. Wang et al., 2014; L. T. Wang et al., 2014), dust (Yang et al.,
70 2013; Y. Wang et al., 2014), and SO_2 (Yang et al., 2013) in Beijing. Atmospheric dynamic
71 processes during hazy conditions were different from clean conditions, with a significant
72 two-way feedback between $\text{PM}_{2.5}$ and boundary layer evolution (Z. Wang et al., 2014).
73 Secondary inorganic aerosol species were suggested to be the major contributor to severe haze,
74 based on off-line $\text{PM}_{2.5}$ analysis (Quan et al., 2014), and on-line non-refractory PM_1 analysis
75 by an Aerosol Chemical Speciation Monitor (Sun et al., 2014). In addition, some studies
76 described unusual atmospheric phenomena taking place under heavily polluted conditions,
77 such as extremely low ozone concentration (less than 5 ppb) in the absence of diurnal

78 variation (Zhao et al., 2013) and the synergistic oxidation of SO₂ and NO₂ (He et al., 2014).
79 These findings suggest need for a better understanding on the haze formation mechanisms.

80 In this study, we address the following questions for the winter haze episodes aforementioned:
81 (1) the relative importance of enhanced emission versus meteorology; (2) the cause of the
82 sharp PM_{2.5} increase during the haze episodes in Beijing, whether it was mainly driven by an
83 extremely rapid local chemical production or by regional transport; and (3) the dominant
84 chemical mechanisms of haze formation.

85

86 **2 Experimental Methods**

87 On-line ambient observation was conducted from 1–31 Jan. 2013 on the campus of Tsinghua
88 University. The observation site is situated on the rooftop of the Environmental Science
89 Building (40°00' 17" N, 116°19' 34" E), approximately 10 m above ground. Tsinghua
90 University is located in the northwest part of urban Beijing, close to the North 4th Ring Road,
91 without any major pollution sources nearby. All observation data are hourly unified data.

92 Mass concentrations of fine (PM_{2.5}) and coarse (PM_{2.5-10}) particles were simultaneously
93 measured based on the β-ray absorption method by a PM-712 Monitor (Kimoto Electric Co.,
94 Ltd., Japan), which was equipped with a US-EPA PM₁₀ inlet and a PM_{2.5} virtual impactor
95 (Kimoto Electric Co., Ltd., 2012; Kaneyasu et al., 2014). Dehumidification was achieved with
96 the hygroscopic growth correction formula:

$$97 \text{ Dehumidified PM}_{2.5} \text{ mass conc.} = \text{Measured PM}_{2.5} \text{ mass conc.} \times \frac{1}{1 + 0.010 \times e^{\frac{6.000 \text{ RH}}{100}}} \quad (1)$$

98 where the 0.010 and 6.000 are localized coefficients, and RH is relative humidity in %. All
99 PM_{2.5} hereinafter refer to the dehumidified PM_{2.5} data.

100 A Sunset Model 4 semi-continuous carbon analyzer (Beaverton, OR, USA) was used to
101 measure hourly organic carbon (OC) and elemental carbon (EC) concentrations in PM_{2.5}. A
102 NIOSH (National Institute for Occupational Safety and Health) temperature protocol was
103 used and the calculation discrepancy under high ambient concentrations was corrected
104 accordingly (G.J. Zheng et al., 2014). Organic matter (OM) was estimated as 1.6*OC, based
105 on previous results (Zhang et al., 2014; Xing et al., 2013). The use of fixed OM/OC ratio

106 requires caveats because the ratio might change due to the variable oxidation degree of OM
107 under different conditions.

108 Hourly sulfate and nitrate concentrations in PM_{2.5} were measured using an ACSA-08 Monitor
109 (Kimoto Electric Co., Ltd., Japan). The ACSA-08 Monitor measured nitrates using a
110 ultra-violet spectrophotometric method, and quantified sulfates with the BaSO₄-based
111 turbidimetric method after addition of BaCl₂ dissolved in polyvinyl pyrrolidone solution
112 (Kimoto et al., 2013). Ammonium was predicted under the assumption that it existed as
113 NH₄NO₃ and (NH₄)₂SO₄ (He et al., 2012), which might be an overestimation based on the
114 non-refractory PM₁ results (Sun et al., 2014). Thus the predicted ammonium given here
115 should be regarded as an upper limit.

116 An automatic meteorological observation instrument (Milos520, VAISALA Inc., Finland)
117 was used to obtain meteorological parameters, including atmospheric pressure, temperature,
118 RH, wind speed, and wind direction. Specific humidity was calculated from these measured
119 parameters (<http://www.srh.noaa.gov/epz/?n=wxcalc>).

120 SO₂ and NO₂ concentrations in Beijing, and PM_{2.5} concentrations in other cities were acquired
121 from the Atmospheric Environment Monitoring Network (Tang et al., 2012). Daily averaged
122 solar radiation reaching ground data were downloaded from the China Meteorological Data
123 Sharing Service System (<http://cdc.cma.gov.cn>). Planetary boundary layer (PBL) height was
124 simulated with the Weather Research & Forecasting (WRF) Model (B. Zheng et al., 2014).

125

126 **3 General Characteristics of Beijing Winter Haze**

127 Primary atmospheric pollutant in Beijing during the winter of 2012–2013 was PM_{2.5}, which
128 constituted about 70% of PM₁₀. This ratio increased when PM_{2.5} pollution became worse (Fig.
129 1b). Monthly average PM_{2.5} concentration reached 121.0 µg/m³ in Jan. 2013, and hourly
130 PM_{2.5} concentrations peaked at 855.10 µg/m³, which was the highest ever reported in Beijing
131 (Zhao et al., 2009; Zhao et al., 2011; Zhao et al., 2013; Zhang et al., 2014). The severe PM_{2.5}
132 pollution lasted nearly the whole month, characterized by frequent and long-lasting pollution
133 episodes. Here, we define an episode as a set of continuous days with daily PM_{2.5} averages
134 exceeding 75 µg/m³. In total, four episodes were identified in Jan. 2013 (Fig. 1a): 4–8 Jan.
135 (Episode I), 10–16 Jan. (Episode II), 18–23 Jan. (Episode III), and 25–31 Jan. (Episode IV).

136 Maximum episode-averaged $PM_{2.5}$ concentrations reached $245.4 \mu\text{g}/\text{m}^3$ in Episode II (see
137 Table 1 for comparative information on Episodes I to III; Episode IV was not included
138 because of missing data). In addition to the high average concentrations, these episodes were
139 frequent (intervals between episodes were all ~ 1 day) and long-lasting (5–7 days) compared
140 with typical durations (5 days) and frequencies (1–3 days) of previous Beijing winter haze
141 episodes (Jia et al., 2008).

142 Another unique feature of the $PM_{2.5}$ mass concentrations during this winter haze period was
143 their dramatic hourly fluctuation. The maximum daily variation was $778.6 \mu\text{g}/\text{m}^3$ on 12 Jan.
144 Hourly $PM_{2.5}$ changes of over $100 \mu\text{g}/\text{m}^3$ (increases or decreases) were observed over 40
145 times during this haze period. Hourly increases or decreases could reach up to $351.8 \mu\text{g}/\text{m}^3$
146 and $-217.7 \mu\text{g}/\text{m}^3$, respectively. Causes of these sharp transitions are discussed in Section 5.

147 The variation of chemical composition with $PM_{2.5}$ pollution level, and among episodes, was
148 also explored. We classified $PM_{2.5}$ pollution into 4 categories according to the Air Quality
149 Index

150 (http://kjs.mep.gov.cn/hjbhbz/bzwb/dqhjbh/jcgfffbz/201203/t20120302_224166.htm?COLLCC=2906016564&) (Fig. 1b): clean ($PM_{2.5} \leq 35 \mu\text{g}/\text{m}^3$), slightly polluted ($35 < PM_{2.5} \leq$
151 $115 \mu\text{g}/\text{m}^3$), polluted ($115 < PM_{2.5} \leq 350 \mu\text{g}/\text{m}^3$), and heavily polluted ($PM_{2.5} > 350 \mu\text{g}/\text{m}^3$),
152 where $PM_{2.5}$ refers to the hourly concentration. Under this classification, the slightly polluted,
153 polluted, and heavily polluted levels generally correspond to small, moderate, and large $PM_{2.5}$
154 peaks in Fig. 1b. Mean percentile compositions of major components in $PM_{2.5}$ under different
155 pollution levels were shown in Fig. 2a. With increasing pollution level, the EC fraction
156 decreased slightly, OC fraction decreased significantly, while sulfate and nitrate contributions
157 increased sharply (Fig. 2a). It suggests that secondary inorganic aerosol species become more
158 important during polluted periods concerning their contribution to the $PM_{2.5}$. A similar trend
159 was observed for NR-PM1 (Sun et al., 2014) and off-line samples (Cheng et al., submitted to
160 Atmos. Environ.). On average, OC, EC, nitrate, and sulfate comprised 21%, 3%, 19% and 22%
161 of $PM_{2.5}$ (Fig. 2b). Good correlations with $PM_{2.5}$ were observed for OC, EC and nitrate ($R^2 >$
162 0.8 for these three species) for all data in Jan. 2013, while for sulfate the correlation became
163 weaker, reflecting larger episodic variations (Fig. 2b). In Episode III, NO_2 exceeded SO_2 by
164 50% (Table 1), generally in accordance with previous studies (Meng et al., 2009). In contrast,
165 concentration of SO_2 exceeded NO_2 in Episodes I and II. Compared with Episode II, Episode
166

167 I was much drier, which is unfavorable to the sulfate formation. The relatively high SO₂ but
168 low NO₂ concentrations in Episodes I and II may indicate the significance of stationary
169 sources (coal combustion, etc.) in local emissions or regional SO₂-rich air masses transported
170 to Beijing.

171

172 **4 Emission Enhancement vs. Synoptic Conditions**

173 Haze episodes were much more severe and frequent in winter 2013 than in 2012. One
174 possible explanation is that there was an abrupt emission enhancement during 2013. However,
175 we didn't find such change in the emission inventory (<http://www.meicmodel.org/>). Annual
176 average emissions of primary PM_{2.5}, SO₂ and NO_x show slight differences between 2013 and
177 2012 (1.2%, -1.3% and 0.8%, respectively) for the Beijing-Tianjin-Hebei region. The changes
178 of monthly averaged emissions in Jan. were higher than the annual average changes in rates,
179 i.e., 2.1%, 1.5% and 2.5% for primary PM_{2.5}, SO₂, and NO_x, respectively; but they are still not
180 significant compared to the changes in pollutant concentrations. Thus, we suspect that these
181 haze episodes arose from the unfavorable synoptic conditions in Jan. 2013.

182 The relative importance of enhanced emission versus unfavorable meteorology in PM_{2.5}
183 concentration of Jan. 2013 was estimated by model simulations with three scenarios (Fig. 3).
184 Base scenario *a* was designed to simulate the actual situation, i.e., with both input emission
185 inventory and meteorology for Jan. 2013. In scenarios *b* and *c*, Jan. 2012 meteorology and Jan.
186 2012 emission inventory data were used, respectively. Since the original WRF-CMAQ
187 (Weather Research and Forecasting - Community Multiscale Air Quality) modeling system
188 cannot reproduce the observed concentrations under heavily polluted conditions (B. Zheng et
189 al. 2014), a revised WRF-CMAQ system with enhanced heterogeneous reactions (Wang et al.,
190 2012) was adopted to improve the model performance. The revised model could effectively
191 capture the measured concentrations of total PM_{2.5} (with normalized mean biases (NMB)
192 being 0.4 %) and its different chemical compositions for both clean and heavily polluted haze
193 days (B. Zheng et al., 2014). Details of the model configuration, modifications, and validation
194 are described in B. Zheng et al. (2014).

195 As expected, the influence of emission difference was negligible (Fig. 3a and 3c). For the
196 whole simulation domain of the North China Plain (NCP), both simulation with Jan. 2012

197 meteorology (Scenario *c*) and Jan. 2013 meteorology (Scenario *a*) resulted in similar PM_{2.5}
198 concentration ranges (~50 to ~500 µg/m³) and spatial distributions. Difference of PM_{2.5}
199 concentration at any site was within ± 10 µg/m³ (Fig. 3e). Simulation results of Scenario *a*
200 and *c* were not only similar in average concentration levels, but also in temporal variations.
201 For example, in Beijing, simulated hourly PM_{2.5} concentration results under this two scenarios
202 presented not only similar concentration (being 279.1 ± 170.2 µg/m³ and 278.8 ± 168.9µg/m³,
203 respectively) but also excellent correlation with R² reaching 0.97.

204 In contrast, stable synoptic conditions in Jan. 2013, which favored accumulation of emitted
205 pollutants, were essential to the formation of the severe regional haze. Under the same
206 emission level, changing the meteorological conditions from 2012 to 2013 resulted in a
207 monthly average PM_{2.5} increase of 10–40 µg/m³ in the Beijing area, and up to 120 µg/m³ over
208 the whole NCP (Fig. 3a, b, d). This suggests that the severe haze episodes in Jan. 2013 were
209 most likely due to unfavorable meteorology, rather than an abrupt increase in emissions (Fig.
210 3d, e).

211 Figure 4 compares peak PM_{2.5} concentrations in the NCP region during Episodes II to IV and
212 their corresponding surface weather maps, together with surface weather map from a clean
213 hour (Fig. 4g). During severe haze episodes, the regional pollution covered most of Hebei
214 Province and northern Henan Province. In general, Shandong Province was less polluted,
215 except during Episode IV. Beijing borders this polluted region, with mountains to the
216 northwest. Surface weather maps from polluted periods were generally characterized by a
217 weak high-pressure center (1034–1037 hPa) northeast of Beijing, which could result in low
218 surface wind speed and prevent the influx of northwest clean air (Xu et al., 2011; Zhao et al.,
219 2013). During the peak hours of Episode II, Beijing was located near a low-pressure trough,
220 where air masses from south, west and northeast converged. During Episode III, Beijing was
221 located in a saddle between two pairs of high- and low-pressure centers, which also led to
222 enhanced stability. In contrast, weather patterns for the clean hours were characterized by
223 strong high-pressure centers (up to 1046 hPa) northwest of Beijing, i.e., the Siberian
224 Anticyclone. With sharp pressure gradient, synoptic conditions produce effective convection
225 and strong northerly winds, bringing dry and clean air masses into Beijing.

226 Local meteorology, controlled by synoptic conditions, could have “deterministic impacts” on
227 air pollution levels (Xu et al., 2011). Compared with the clean periods, the polluted periods

228 were associated with significantly lower wind speed and PBL, and higher temperature and RH
229 (Fig. 5). Besides changes in the average level, diurnal pattern of temperature in polluted
230 periods could also differ from clean periods, with diminished overnight (0:00 to 6:00 a.m.)
231 temperature drop.

232

233 **5 Local Chemical Production vs. Regional Transport**

234 As shown in Fig. 6, Episode II consists of several sharp-increase events, in which $PM_{2.5}$
235 concentrations increased by over $400 \mu\text{g}/\text{m}^3$ within 1–3 hours (maximum mass growth rate up
236 to $351.8 \mu\text{g}/\text{m}^3/\text{h}$). Earlier studies have attributed this dramatic rate of increase to fast local
237 chemical production (Y. Wang et al., 2014). However, we found that the apparent rapid
238 changes are more likely to be caused by the regional transport of clean/polluted air masses. In
239 winter, the Siberian Anticyclone could bring clean air masses into NCP (Jia et al., 2008; Liu
240 et al., 2013) while southerly winds refill the areas with polluted air masses. The transition
241 between clean and polluted air masses may result in an apparent sharp build-up of particle
242 concentrations. In other words, these events reflected interruption and rapid recovery of
243 pollution from adjacent areas, rather than merely local chemical production.

244 The impact of transport is supported by the temporal variations in the regional distribution of
245 $PM_{2.5}$ concentrations, the surface weather maps, and the specific humidity (Fig. 6 and 7). The
246 first evidence is that these sharp $PM_{2.5}$ build-up events were unique to Beijing among all the 8
247 cities around/in the NCP (Fig. 6). Chengde and Zhangjiakou are situated to the north of NCP
248 with mountains in between (Fig. 6a). Among the NCP cities, Beijing is located at the northern
249 tip, with mountains to the north and west shielding the city (Fig. 6 (a2)). When conditions
250 favor transport of clean air from north or northwest (i.e. with the advent of a cold air current),
251 Beijing is the first one among NCP cities to be scavenged, which resulted in a sharp drop of
252 $PM_{2.5}$ concentrations. In this case, $PM_{2.5}$ levels in Beijing became similar to the upwind cities,
253 i.e., Chengde and Zhangjiakou (yellow solid circles; Fig. 6(b1)). However, these cold air
254 currents were too weak to go further, leaving the rest NCP cities unaffected. Not surprisingly,
255 the influence of these weak cold air currents soon receded and the polluted air parcels were
256 transported back to Beijing, which lead to a sharp increase in the $PM_{2.5}$ level similar as the

257 rest NCP cities (e.g., Shijiazhuang, Baoding, Tianjin, Langfang, and Tangshan) (yellow solid
258 circles; Fig. 6 (b2 and b3)).

259 In accordance with the above description, surface weather maps showed that the sharp $PM_{2.5}$
260 increase/decrease events in Beijing during Jan. 2013 were always accompanied with quick
261 transition between low/high pressure systems. As shown in Fig. 7b, the two sharp drops in
262 $PM_{2.5}$ concentration on 11 and 12 Jan. corresponded to a weak high-pressure system
263 developed in the mountains northwest of Beijing, which brought clean air mass into the city.
264 When the high-pressure systems diminished, a low-pressure system developed southwest of
265 Beijing, and the air mass in Beijing was again affected by the regional background pollution,
266 resulting in a sharp increase in $PM_{2.5}$ concentration.

267 The observed variation of the specific humidity, an indicator for the origin of air masses (Jia
268 et al., 2008), also supports our explanation (Fig. 7a). Air masses from the south were usually
269 warmer and wetter than the northern air masses, thus possessing a higher specific humidity.
270 During the rapid changes of $PM_{2.5}$, the trend of specific humidity nicely followed the
271 variations of $PM_{2.5}$ (Fig. 7a, pink and yellow rectangles marked periods), which reflected the
272 quick transition of air parcel origins. It has been suggested that the decrease of PBL height
273 will compress air pollutants into a shallow layer, resulting in elevated pollution levels (Liu et
274 al., 2013). However, our results indicated that the compression was not really happening.
275 Rather, the decrease of PBL height hindered the vertical mixing of pollutants, resulting in a
276 faster accumulation and higher concentrations. As shown in Fig. 7a, the time lag between
277 variations in PBL and its effects on $PM_{2.5}$ concentration is a clear evidence demonstrating that
278 the PBL was not “compressing” air pollutants into a shallower layer. Otherwise, concurrent
279 increase in $PM_{2.5}$ will be found during the decrease of PBL height.

280

281 **6 Formation of Secondary Aerosols**

282 Compared with clean conditions, the hazy days are characteristic of weaker radiation and
283 higher RH. The RH depends on the synoptic conditions while the radiation reduction is due to
284 the direct radiative effects of aerosol particles (Crutzen and Birks, 1982; Ramanathan and
285 Carmichael, 2008; Ramanathan et al., 2001; Cheng et al., 2008b; Wendisch et al., 2008).
286 Secondary aerosols (inorganic and organic) are major components in fine particles in China

287 (Yang et al., 2011). In this section, we will evaluate the impact of changes in radiation and
288 RH on the formation of secondary aerosols.

289 To evaluate the role of chemical productions, we analyzed the EC-scaled concentrations for
290 individual compounds. The purpose of using EC-scaled concentration is to eliminate the
291 influence of different dilution/mixing conditions on the variation of observed pollutant
292 concentrations. The observed variations of pollutant concentrations are not only controlled by
293 the chemical reactions but also subject to the influence of boundary layer developments. For
294 the same emission rate and chemical production rate, different mixing conditions will result in
295 different level of air pollutants. It is thus highly uncertain to conclude a stronger/weaker
296 chemical production based on purely concentrations data without considering the boundary
297 layer effect. Since EC is an aerosol species coming from only primary emission and quite
298 inertial to chemical reactions, its variations well reflect the influence of atmospheric physical
299 processes (dilution/mixing effect). The ratio of other species to EC will to a large extent
300 eliminate the variations due to mixing/dilution and better represent the contribution from
301 chemical reactions.

302 **6.1 Weakened Importance of Photochemistry**

303 The radiative reduction imposed by aerosol particles is particularly strong during haze
304 episodes because of extremely high particle concentrations. Take Beijing for example, during
305 haze episodes, the amount of solar radiation reaching the ground was significantly lower (e.g.,
306 down to 2.77 MJ/m²/day, 13 Jan.) than clean days (averaging 9.36 ± 0.60 MJ/m²/day for all
307 the six clean days), rendering high photochemical activity impossible. The reduction of
308 radiation intensities will change the atmospheric photochemistry and oxidant concentrations
309 (hydroxyl radical (OH) and ozone (O₃)), which will consequently change the production and
310 aging of secondary organic aerosols (SOA) (Hallquist et al., 2009; Jimenez et al., 2009).

311 As the haze pollution spread over most of the NCP, a weakening of photochemistry was
312 expected on the regional scale, which is confirmed by both observations and model
313 simulations. Extremely low ozone concentration (less than 10 ppb) in the absence of diurnal
314 variation was observed during heavy pollution episodes for all of the three major cities in
315 Jing-Jin-Ji Area (i.e., Beijing, Tianjin and Shijiazhuang) in Jan. 2013 (Y. Wang et al., 2014).
316 Similar phenomenon was observed before in another heavy pollution episode in winter

317 Beijing (Zhao et al., 2013). In accordance with the observed low ozone concentration, model
318 simulations also showed a regional-scale reduction in the concentrations of ozone and OH
319 (Fig. 8). Average daytime concentrations of oxidants were significantly lower during polluted
320 periods than clean periods. For most areas in the NCP, O₃ and OH dropped from 12~44 ppbV
321 and 0.004 ~ 0.020 pptV to less than 12 ppbV and 0.004 pptV, respectively, as the air quality
322 changed from clean to heavily polluted conditions. This regional drop in oxidant
323 concentrations demonstrates the impact of air pollution on the photochemistry.

324 Ozone and OH radicals are known as crucial oxidants in the formation of secondary organics
325 aerosols (SOA) (Jimenez et al. 2009). Weakened photochemistry is therefore expected to
326 reduce the SOA production and concentrations. To have a semi-quantitative estimation on the
327 contribution of photochemistry, secondary organic carbon (SOC) was estimated (Fig. 9a)
328 using the EC-tracer method (Lim and Turpin, 2002). Briefly, SOC was estimated using these
329 formulae:

$$330 \quad \text{Primary OC} = \text{EC} * (\text{OC/EC})_{\text{pri}} + \text{N} \quad (2)$$

$$331 \quad \text{SOC} = \text{OC} - \text{Primary OC} \quad (3)$$

332 The basic assumptions and underlying principles of this method are discussed in Lim and
333 Turpin (2002) and Lin et al. (2009). Only daytime (7:00~18:00) carbonaceous aerosol data
334 were used here to exclude possible interference from day-night source variations (such as the
335 heavy-duty diesel truck traffic which is allowed only during nighttime in Beijing). In our
336 study, data pairs with the lowest 10% percentile of ambient OC/EC ratios were used to
337 estimate the primary OC/EC ratio (Fig. 9a). York regression (York et al., 2004) was used to
338 estimate the intercept N and the slope, i.e., values of (OC/EC) pri, according to Saylor et al.
339 (2006). Our analysis shows that SOC constituted ~28% of total OC, consistent with earlier
340 studies in the winter of 2009-2012 (~30%, Cheng et al., 2011; Sun et al., 2013b).

341 High concentration of aerosol particles can reduce solar radiation and atmospheric
342 photochemistry. Since SOC is a product of photochemical reactions, we would expect a
343 reduced SOC production rate under heavily polluted conditions. This is confirmed by the
344 measured SOC concentrations shown in Fig. 9. Here again the EC-scaled SOC was used to
345 account for the different boundary layer effect (dilution/mixing) on the aerosol concentrations.
346 Both SOC/EC and the accumulated SOC/EC (afternoon – morning values) decrease when it

347 changed from clean to heavily polluted periods. The accumulated SOC/EC is used to better
348 represent the production during the daytime.

349 Reduction in photochemistry-related $PM_{2.5}$ production is further supported by model
350 simulation results. In our model configurations, the photolysis rate is calculated online using
351 simulated aerosols and ozone concentrations (B. Zheng et al., 2014). As a result, with the
352 enhanced $PM_{2.5}$ concentration, the photolysis rate will be reduced, and so will the
353 concentrations of photochemical oxidants (Fig. 8) and secondary aerosol particles. During the
354 haze events, this effect can be counteracted by the enhanced heterogeneous reactions and it is
355 difficult to unravel them from the measurement data.

356 In order to demonstrate the influence of reduced photochemistry, we adopted the original
357 WRF-CMAQ model setup and excluded the enhanced heterogeneous reactions. In this case,
358 only gas phase oxidations are counted for the formation of sulfate and organics
359 (aqueous-phase reactions in the original WRF-CMAQ only happen in clouds and don't apply
360 for the aerosol phase) (B. Zheng et al., 2014) and their simulated concentrations will directly
361 reflect the influence of reduced photochemistry. As shown in Table S1, the simulated
362 $PM_{2.5}/EC$ ratios decreased from 16.05 to 11.72 when the pollution level changed from the
363 clean to the heavily polluted case, reflecting the reduced gas-phase photochemical production.
364 Note that $PM_{2.5}$ concentration is normalized by EC to counteract the influence of reduced
365 boundary layer. Otherwise, the reduced boundary layer itself could lead to a tremendous
366 increase in the pollutant concentration under heavily polluted conditions, and thus cover the
367 real effect of reduced photochemistry.

368 The simulated individual components of $PM_{2.5}$ also reflected the influence of photochemistry.
369 As shown in Table S1, although primary organic matter (POM) to EC ratios kept nearly
370 constant during all pollution levels, the normalized secondary species all showed a decreasing
371 trend, reflecting the reduced photochemical production. SOA/EC , SO_4^{2-}/EC , and NO_3^-/EC
372 ratios decreased by 53.3%, 51.9% and 28.6%, respectively from clean to heavily polluted
373 periods. For the formation of NO_3^- , two heterogeneous reactions have been included in the
374 original WRF-CMAQ model and therefore the NO_3^-/EC shows relatively less reduction than
375 SOA/EC and SO_4^{2-}/EC .

376

377 **6.2 Enhanced Heterogeneous Chemistry**

378 Unlike OM, relative contributions of sulfate and nitrate to $PM_{2.5}$ were increasing during the
379 haze events (Fig. 2). Again, we used their ratios to EC to account for the boundary layer effect.
380 An increasing trend of SO_4^{2-}/EC and NO_3^-/EC ratios was found (Column 1 in Fig. 10) from
381 clean periods (3.03 and 3.33, respectively) to heavily polluted periods (6.35 and 5.89,
382 respectively), suggesting enhanced chemical productions. The SOR and NOR (molar ratio of
383 sulfate or nitrate to sum of sulfate and SO_2 or nitrate and NO_2) have been used as indicators of
384 secondary transformation (Sun et al., 2006). The fact that SOR and NOR increased much
385 more rapidly than SO_2 and NO_2 as pollutions became more severe (Column 4 in Fig. 10), is
386 another evidence of elevated secondary formations of sulfate and nitrate during severe haze
387 events.

388 Both gas-phase and heterogeneous reactions could contribute to the formation of sulfate and
389 nitrate from SO_2 and NO_2 , and thus elevating the SOR and NOR. Sulfate is formed through
390 oxidation of SO_2 by gas-phase reactions with OH (Stockwell and Calvert, 1983; Blitz et al.,
391 2003) and stabilized Criegee intermediate (which is formed by O_3 and alkenes) (Mauldin et
392 al., 2012), and by heterogeneous reactions with dissolved H_2O_2 or with O_2 under the catalysis
393 of transition metal (Seinfeld and Pandis, 2006). Nitrate formation is dominated by the
394 gas-phase reaction of NO_2 with OH during daylight, and the heterogeneous reactions of
395 nitrate radical (NO_3) during nighttime (Seinfeld and Pandis, 2006). Since gas phase
396 production of secondary aerosols is expected to decrease under heavily polluted periods
397 (Section 6.1), the increase of SO_4^{2-}/EC and NO_3^-/EC ratios is a clear evidence for the
398 dominant contribution from other pathways, most probably from the heterogeneous reactions.

399 If we assume heterogeneous chemistry as answer to the high SO_4^{2-} and NO_3^- concentrations,
400 there is a problem because heterogeneous chemistry still requires oxidation by oxidizing
401 agents, e.g. OH, O_3 , etc., which were indeed significantly reduced (Section 6.1). Our
402 explanation for this puzzle is that despite of reduced oxidant concentrations, the aerosol
403 volume/surface increases so much (due to elevated aerosol concentration and the
404 accompanied high RH, Fig. 1) that it is enough to compensate its influence, and moreover,
405 leads to a net increase in the formation of secondary aerosols.

406 A simplified case study could show how aerosol volume/surface increases could compensate
 407 the effect of oxidant reduction, and even lead to a net increase in the formation of secondary
 408 aerosols. Take sulfate for example, the production rate of sulfate (S(VI)) through
 409 heterogeneous reactions can be estimated by:

$$410 \quad dC_{S(VI)}/dt \approx k[S(IV)(aq)] * [\text{oxidants}(aq)] * V_{\text{aerosol}} \quad (4)$$

411 in which $C_{S(VI)}$ is the sulfate concentration, k is the effective rate coefficient, $[S(IV)(aq)]$ is the
 412 S(IV) concentration in the aqueous phase of aerosols, $[\text{oxidants}(aq)]$ is the concentration of
 413 oxidants in the aqueous phase of aerosols, and V_{aerosol} is the volume concentration of
 414 humidified aerosol at ambient RH.

415 Equation (4) shows that the oxidants and V_{aerosol} are both essential for the heterogeneous
 416 reactions. From the clean to the heavily polluted case, O_3 is reduced by 80%, dropping from >
 417 $50 \mu\text{g}/\text{m}^3$ to $< 10 \mu\text{g}/\text{m}^3$ (Y. Wang et al., 2014). Based on our model simulation results, H_2O_2
 418 concentration also dropped significantly from ~ 78 ppbV to ~ 11 ppbV. Thus we assume an
 419 upper limit of 90% reduction in $[\text{oxidants}(aq)]$. V_{aerosol} depends on the dry aerosol
 420 concentrations V_{dry} and its hygroscopic growth factor (GF) of particle size, which is a function
 421 of RH. Assuming a constant aerosol dry density, then V_{dry} is proportional to the mass
 422 concentration. From clean to heavily polluted case, average $PM_{2.5}$ mass concentration
 423 increased by 25 time, changing from $18 \mu\text{g}/\text{m}^3$ to $450 \mu\text{g}/\text{m}^3$ while average RH increased from
 424 dry ($\sim 20\%$) to $\sim 70\%$. Thus we have:

$$425 \quad \frac{[\text{oxidants}(aq)]_{HP} * (V_{\text{aerosol}})_{HP}}{[\text{oxidants}(aq)]_{Clean} * (V_{\text{aerosol}})_{Clean}} = \frac{[\text{oxidants}(aq)]_{HP}}{[\text{oxidants}(aq)]_{Clean}} * \frac{(V_{\text{dry}})_{HP}}{(V_{\text{dry}})_{Clean}} * (GF_{HP/Clean})^3 \approx 0.1 * 25 * (1.1)^3 = 3.33 \quad (5)$$

426 where HP and Clean indicated heavily polluted and clean periods, respectively. A GF of 1.1
 427 was taken from previous measurements in Beijing (Meier et al., 2009).

428 Equation (5) shows that the increase of aerosol volume concentrations could sufficiently
 429 compensate the effect of oxidant reduction, resulting in a net increase of sulfate production.

430 Similarly, for NO_3^- , the influence of oxidant reduction could also be compensated by the
 431 increase of aerosol volume concentrations. There might be other oxidants associated with
 432 heterogeneous reactions, such as O_2 (especially under the catalysis of mineral metals) and
 433 other oxidants existed in aerosol phase such as Organic Peroxides (Seinfeld et al., 2006).

434 In accordance with above discussions, both observation and model simulation supported the
435 importance of heterogeneous reactions. Observed SOR and NOR showed an obvious
436 dependence on RH (Fig. 11). Both SOR and NOR were constant under dry conditions (RH <
437 50%) (Fig. 11 a, b) while started increasing when RH >50%, resulting in average values
438 around 0.34 and 0.28 at RH 70%–80%, respectively. This suggests important contributions
439 from heterogeneous reactions with abundant aerosol water under wet conditions (Sun et al.,
440 2013a). The observed SOR value was high compared with previously reported values of 0.24
441 (Wang et al., 2006) and 0.29 (Zhao et al., 2013) during hazy days in Beijing. The NOR value
442 for this study was higher than for spring hazy days in 2001–2004 (0.22; Wang et al., 2006),
443 but significantly lower than for the hazy episode in Jan. 2010 (0.51; Zhao et al., 2013). Our
444 model simulation results (B. Zheng et al., 2014) also supported the importance of
445 heterogeneous chemistry in sulfate and nitrate productions (Figure R1). With the addition of
446 the heterogeneous reactions, the revised CMAQ showed much better performance in the
447 polluted periods (B. Zheng et al., 2014), which demonstrated the importance of heterogeneous
448 reaction in the production of secondary aerosols.

449 Concerning the SOA formation, the contribution of heterogeneous reactions might be possible,
450 but it should be much less significant than for sulfate and nitrate. For RH > 50%, $\text{SO}_4^{2-}/\text{EC}$
451 and NO_3^-/EC ratios rose significantly (Fig. 11d) while SOC/EC ratios remained constant (Fig.
452 9b). By using HOA (hydrocarbon-like organic aerosol) instead of EC, Sun et al. (2013a)
453 found similar phenomena. Apparently, SOC doesn't have a heterogeneous formation pathway
454 as effective as those of sulfate and nitrate.

455

456 **7 Conclusion**

457 The severe haze pollution during Jan. 2013 was not a Beijing-localized phenomenon. Rather,
458 it was the result of local pollutants superposed on background regional pollution, which
459 affected the whole NCP. Although pollutant emissions were high, there was no abrupt
460 enhancement in 2013. The occurrence of the severe winter haze resulted from stable synoptic
461 meteorological conditions over a large area of northeastern China. Surface weather maps from
462 hazy periods were characterized by a weak high-pressure center northeast of Beijing, while
463 the termination of a haze episode was always accompanied by the Siberian Anticyclone (Xu

464 et al., 2011; Jia et al., 2008; Liu et al., 2013). Atmospheric chemistry and physics during
465 severe haze pollutions are illustrated in a conceptual model (Fig. 12). With the onset of stable
466 synoptic conditions, RH rises, primary pollutants begin to accumulate and regional pollution
467 begins to form. If the stable conditions last long enough, PM_{2.5} build-up occurs, and as a
468 consequence, solar radiation is reduced at the ground level. This inhibits surface temperature
469 fluctuation, making easier the formation of inversed layer and rendering the atmosphere into a
470 more stable condition. Meanwhile, photochemical activity is weakened under low solar
471 radiation, and secondary aerosol formation via this pathway becomes less important. However,
472 under high RH, heterogeneous reactions may play a more important role, especially those
473 associated with the aerosol aqueous phase. This results in the rapid build-up of secondary
474 aerosols, especially sulfates and nitrates, enhancing PM_{2.5} pollution. The accumulation of
475 aerosol particles terminates with the incursion of a strong cold front, usually the Siberian
476 Anticyclone.

477 Our analysis also reveals that the regional transport can be a key process controlling the
478 variations of local air pollutant concentrations. Take the sharp increases of aerosols
479 concentrations on 11-13 Jan. for example, Beijing pollution was temporarily flushed away by
480 strong winds associated with the arrival of a weak cold air current, as its influence weakened,
481 the polluted regional air mass readily reoccupied the Beijing area, resulting in an apparent
482 rapid build-up of PM_{2.5}. This was supported by data on the PM_{2.5} levels around Beijing,
483 specific humidity and PBL height, as well as surface weather maps. Our results reveal that the
484 apparent formation rate (the rate of change in PM_{2.5} or other air pollutants) is not only due to
485 chemical reactions but also controlled by the regional transport along with other processes. It
486 requires caveats to derive a real chemical production rate based on a single-site measurement.
487 Our results also show a clear impact of regional transport on the local air pollution, suggesting
488 the importance of regional-scale emission control measures in the local air quality
489 management of Beijing.

490

491

492 **Acknowledgments**

493 This work was supported by the National Natural Science Foundation of China (21190054,
494 21221004, 21107061, 41222036 and 41330635), China's National Basic Research Program
495 (2010CB951803), and the Japan International Cooperation Agency. F. K. Duan acknowledges
496 support from a National Excellent Doctoral Dissertation of China Award (2007B57). Y.
497 Cheng was supported by the China Postdoctoral Science Foundation (2013T60130 and
498 2013M540104). D. Chang, H. Su and Y. F. Cheng were supported by the Max Planck Society
499 (MPG) and the EU project PEGASOS (265148).
500

501 **References**

502 Blitz, M. A., Hughes, K. J., and Pilling, M. J.: Determination of the high-pressure limiting
503 rate coefficient and the enthalpy of reaction for OH+SO₂, *J. Phys. Chem. A*, 107, 1971-1978,
504 doi:10.1021/jp026524y, 2003.

505 Cao, C., Jiang, W., Wang, B., Fang, J., Lang, J., Tian, G., Jiang, J., and Zhu, T. F.: Inhalable
506 Microorganisms in Beijing's PM_{2.5} and PM₁₀ Pollutants during a Severe Smog Event,
507 *Environ. Sci. Technol.*, 48, 1499-1507, 2014.

508 Carmichael, G. R., Streets, D. G., Calori, G., Amann, M., Jacobson, M. Z., Hansen, J., and
509 Ueda, H.: Changing trends in sulfur emissions in Asia: Implications for acid deposition, air
510 pollution, and climate, *Environ. Sci. Technol.*, 36, 4707-4713, doi:10.1021/es011509c, 2002.

511 Chan, C. K., and Yao, X.: Air pollution in mega cities in China, *Atmos. Environ.*, 42, 1-42,
512 2008.

513 Chen, Y., Sheng, G., Bi, X., Feng, Y., Mai, B., and Fu, J.: Emission factors for carbonaceous
514 particles and polycyclic aromatic hydrocarbons from residential coal combustion in China,
515 *Environ. Sci. Technol.*, 39, 1861-1867, 2005.

516 Cheng, Y. F., Eichler, H., Wiedensohler, A., Heintzenberg, J., Zhang, Y. H., Hu, M.,
517 Herrmann, H., Zeng, L. M., Liu, S., Gnauk, T., Brüggemann, E., and He, L. Y.: Mixing state
518 of elemental carbon and non-light-absorbing aerosol components derived from in situ particle
519 optical properties at Xinken in Pearl River Delta of China, *J. Geophys. Res.*, 111, doi:
520 10.1029/2005JD006929, 2006.

521 Cheng, Y. F., Heintzenberg, J., Wehner, B., Wu, Z. J., Su, H., Hu, M., and Mao, J. T.: Traffic
522 restrictions in Beijing during the Sino-African Summit 2006: aerosol size distribution and
523 visibility compared to long-term in situ observations, *Atmos. Chem. Phys.*, 8, 7583-7594,
524 doi:10.5194/acp-8-7583-2008, 2008a.

525 Cheng, Y., Wiedensohler, A., Eichler, H., Heintzenberg, J., Tesche, M., Ansmann, A.,
526 Wendisch, M., Su, H., Althausen, D., and Herrmann, H.: Relative humidity dependence of
527 aerosol optical properties and direct radiative forcing in the surface boundary layer at Xinken
528 in Pearl River Delta of China: An observation based numerical study, *Atmos. Environ.*, 42,
529 6373-6397, 2008b.

530 Cheng, Y. F., Wiedensohler, A., Eichler, H., Su, H., Gnauk, T., Brüggemann, E., Herrmann,
531 H., Heintzenberg, J., Slanina, J., Tuch, T., Hu, M., and Zhang, Y. H.: Aerosol optical
532 properties and related chemical apportionment at Xinken in Pearl River Delta of China,
533 *Atmos. Environ.*, 42, 6351-6372, doi:10.1016/j.atmosenv.2008.02.034, 2008c.

534 Cheng, Y., He, K.-b., Duan, F.-k., Zheng, M., Du, Z.-y., Ma, Y.-l., and Tan, J.-h.: Ambient
535 organic carbon to elemental carbon ratios: Influences of the measurement methods and
536 implications, *Atmos. Environ.*, 45, 2060-2066, doi: 10.1016/j.atmosenv.2011.01.064, 2011.

537 Crutzen, P. J., and Birks, J. W.: Atmosphere after a nuclear war: Twilight at noon, *Ambio*
538 (Allen Press), 11 (2/3), 114–125, 1982.

539 Docherty, K. S., Stone, E. A., Ulbrich, I. M., DeCarlo, P. F., Snyder, D. C., Schauer, J. J.,
540 Peltier, R. E., Weber, R. J., Murphy, S. M., Seinfeld, J. H., Grover, B. D., Eatough, D. J., and
541 Jimenez, J. L.: Apportionment of Primary and Secondary Organic Aerosols in Southern
542 California during the 2005 Study of Organic Aerosols in Riverside (SOAR-1), *Environ. Sci.*
543 *Technol.*, 42, 7655-7662, doi:10.1021/es8008166, 2008.

544 Duan, J., Tan, J., Yang, L., Wu, S., and Hao, J.: Concentration, sources and ozone formation
545 potential of volatile organic compounds (VOCs) during ozone episode in Beijing, *Atmos.*
546 *Res.*, 88, 25-35, doi:10.1016/j.atmosres.2007.09.004, 2008.

547 Hallquist, M., Wenger, J. C., Baltensperger, U., Rudich, Y., Simpson, D., Claeys, M.,
548 Dommen, J., Donahue, N. M., George, C., Goldstein, A. H., Hamilton, J. F., Herrmann, H.,
549 Hoffmann, T., Iinuma, Y., Jang, M., Jenkin, M. E., Jimenez, J. L., Kiendler-Scharr, A.,
550 Maenhaut, W., McFiggans, G., Mentel, T. F., Monod, A., Prévôt, A. S. H., Seinfeld, J. H.,
551 Surratt, J. D., Szmigielski, R., and Wildt, J.: The formation, properties and impact of
552 secondary organic aerosol: current and emerging issues, *Atmos. Chem. Phys.*, 9, 5155-5236,
553 doi:10.5194/acp-9-5155-2009, 2009.

554 He, H., Wang, Y., Ma, Q., Ma, J., Chu, B., Ji, D., Tang, G., Liu, C., Zhang, H., and Hao, J.:
555 Mineral dust and NO_x promote the conversion of SO₂ to sulfate in heavy pollution days, *Sci.*
556 *Rep.*, 4, 4172, doi:10.1038/srep04172, 2014.

557 He, K., Zhao, Q., Ma, Y., Duan, F., Yang, F., Shi, Z., and Chen, G.: Spatial and seasonal
558 variability of PM_{2.5} acidity at two Chinese megacities: insights into the formation of

559 secondary inorganic aerosols, *Atmos. Chem. Phys.*, 12, 1377-1395, doi:
560 10.5194/acp-12-1377-2012, 2012.

561 Jia, Y., Rahn, K. A., He, K., Wen, T., and Wang, Y.: A novel technique for quantifying the
562 regional component of urban aerosol solely from its sawtooth cycles, *J. Geophys. Res.*, 113,
563 D21309, doi:10.1029/2008jd010389, 2008.

564 Jimenez, J. L., Canagaratna, M. R., Donahue, N. M., Prevot, A. S. H., Zhang, Q., Kroll, J. H.,
565 DeCarlo, P. F., Allan, J. D., Coe, H., Ng, N. L., Aiken, A. C., Docherty, K. S., Ulbrich, I. M.,
566 Grieshop, A. P., Robinson, A. L., Duplissy, J., Smith, J. D., Wilson, K. R., Lanz, V. A.,
567 Hueglin, C., Sun, Y. L., Tian, J., Laaksonen, A., Raatikainen, T., Rautiainen, J., Vaattovaara,
568 P., Ehn, M., Kulmala, M., Tomlinson, J. M., Collins, D. R., Cubison, M. J., Dunlea, E. J.,
569 Huffman, J. A., Onasch, T. B., Alfarra, M. R., Williams, P. I., Bower, K., Kondo, Y.,
570 Schneider, J., Drewnick, F., Borrmann, S., Weimer, S., Demerjian, K., Salcedo, D., Cottrell,
571 L., Griffin, R., Takami, A., Miyoshi, T., Hatakeyama, S., Shimono, A., Sun, J. Y., Zhang, Y.
572 M., Dzepina, K., Kimmel, J. R., Sueper, D., Jayne, J. T., Herndon, S. C., Trimborn, A. M.,
573 Williams, L. R., Wood, E. C., Middlebrook, A. M., Kolb, C. E., Baltensperger, U., and
574 Worsnop, D. R.: Evolution of Organic Aerosols in the Atmosphere, *Science*, 326, 1525-1529,
575 doi:10.1126/science.1180353, 2009.

576 Kaneyasu, N., Yamamoto, S., Sato, K., Takami, A., Hayashi, M., Hara, K., Kawamoto, K.,
577 Okuda, T., and Hatakeyama, S.: Impact of long-range transport of aerosols on the PM_{2.5}
578 composition at a major metropolitan area in the northern Kyushu area of Japan, *Atmos.*
579 *Environ.*, doi:10.1016/j.atmosenv.2014.01.029, in press, 2014.

580 Khalil, M. A. K. and Rasmussen, R. A.: Tracers of wood smoke, *Atmos. Environ.*, 37, 1211–
581 1222, doi:10.1016/s1352-2310(02)01014-2, 2003.

582 Kimoto Electric Co., Ltd.: Technical Notes for Continuous Measuring Methods for
583 Atmospheric Suspended Particulate Matters, 3rd edn., March 2012, Osaka, Japan, 2012 (in
584 Japanese).

585 Kimoto, H., Ueda, A., Tsujimoto, K., Mitani, Y., Toyazaki, Y., and Kimoto, T.: Development
586 of a Continuous Dichotomous Aerosol Chemical Speciation Analyzer, *Clean Technology*, 23,
587 49–52, 2013 (in Japanese).

588 Li, W. and Shao, L.: Transmission electron microscopy study of aerosol particles from the
589 brown hazes in northern China, *J. Geophys. Res.-Atmos.*, 114, D09302,
590 doi:10.1029/2008jd011285, 2009.

591 Lim, H.-J., and Turpin, B. J.: Origins of primary and secondary organic aerosol in Atlanta:
592 Results of time-resolved measurements during the Atlanta supersite experiment, *Environ. Sci.*
593 *Technol.*, 36, 4489-4496, 2002.

594 Lin, P., Hu, M., Deng, Z., Slanina, J., Han, S., Kondo, Y., Takegawa, N., Miyazaki, Y., Zhao,
595 Y., and Sugimoto, N.: Seasonal and diurnal variations of organic carbon in PM_{2.5} in Beijing
596 and the estimation of secondary organic carbon, *J. Geophys. Res.*, 114, D00G11,
597 doi:10.1029/2008jd010902, 2009.

598 Liu, X. G., Li, J., Qu, Y., Han, T., Hou, L., Gu, J., Chen, C., Yang, Y., Liu, X., Yang, T.,
599 Zhang, Y., Tian, H., and Hu, M.: Formation and evolution mechanism of regional haze: a case
600 study in the megacity Beijing, China, *Atmos. Chem. Phys.*, 13, 4501-4514,
601 doi:10.5194/acp-13-4501-2013, 2013.

602 Lu, K. D., Hofzumahaus, A., Holland, F., Bohn, B., Brauers, T., Fuchs, H., Hu, M., Häseler,
603 R., Kita, K., Kondo, Y., Li, X., Lou, S. R., Oebel, A., Shao, M., Zeng, L. M., Wahner, A.,
604 Zhu, T., Zhang, Y. H., and Rohrer, F.: Missing OH source in a suburban environment near
605 Beijing: observed and modelled OH and HO₂ concentrations in summer 2006, *Atmos. Chem.*
606 *Phys.*, 13, 1057-1080, doi:10.5194/acp-13-1057-2013, 2013.

607 Mauldin, R. L., Berndt, T., Sipila, M., Paasonen, P., Petaja, T., Kim, S., Kurten, T., Stratmann,
608 F., Kerminen, V. M., and Kulmala, M.: A new atmospherically relevant oxidant of sulphur
609 dioxide, *Nature*, 488, 193-196, doi:10.1038/nature11278, 2012.

610 Meier, J., Wehner, B., Massling, A., Birmili, W., Nowak, A., Gnauk, T., Brüeggemann, E.,
611 Herrmann, H., Min, H., and Wiedensohler, A.: Hygroscopic growth of urban aerosol particles
612 in Beijing (China) during wintertime: a comparison of three experimental methods, *Atmos.*
613 *Chem. Phys.*, 9, 6865-6880, doi:10.5194/acp-9-6865-2009, 2009.

614 Meng, Z. Y., Xu, X. B., Yan, P., Ding, G. A., Tang, J., Lin, W. L., Xu, X. D., and Wang, S. F.:
615 Characteristics of trace gaseous pollutants at a regional background station in Northern China,
616 *Atmos. Chem. Phys.*, 9, 927-936, 2009.

617 Nel, A.: Air pollution-related illness: effects of particles, *Science*, 308, 804-806, 2005.

618 Ouyang, Y.: China wakes up to the crisis of air pollution, *The Lancet Respiratory Medicine*, 1,
619 20 p. 12, doi:10.1016/S2213-2600(12)70065-6, 2013.

620 Peplow, M.: Beijing smog contains witches' brew of microbes, *Nature*,
621 doi:10.1038/nature.2014.14640, 2014.

622 Pöschl, U.: Atmospheric aerosols: Composition, transformation, climate and health effects,
623 *Angew. Chem. Int. Edit.*, 44, 7520-7540, 2005.

624 Plaza, J., Gomez-Moreno, F. J., Nunez, L., Pujadas, M., and Artinano, B.: Estimation of
625 secondary organic aerosol formation from semicontinuous OC-EC measurements in a Madrid
626 suburban area, *Atmos. Environ.*, 40, 1134-1147, doi:10.1016/j.atmosenv.2005.11.007, 2006.

627 Quan, J., Tie, X., Zhang, Q., Liu, Q., Li, X., Gao, Y., and Zhao, D.: Characteristics of heavy
628 aerosol pollution during the 2012–2013 winter in Beijing, China, *Atmos. Environ.*, 88, 83-89,
629 doi:10.1016/j.atmosenv.2014.01.058, 2014.

630 Ramanathan, V., Crutzen, P. J., Lelieveld, J., Mitra, A., Althausen, D., Anderson, J., Andreae,
631 M., Cantrell, W., Cass, G., and Chung, C.: Indian Ocean Experiment: An integrated analysis
632 of the climate forcing and effects of the great Indo - Asian haze, *J. Geophys. Res.*, 106,
633 28371-28398, 2001.

634 Ramanathan, V., and Carmichael, G.: Global and regional climate changes due to black
635 carbon, *Nat. Geosci.*, 1, 221-227, 2008.

636 Saylor, R. D., Edgerton, E. S., and Hartsell, B. E.: Linear regression techniques for use in the
637 EC tracer method of secondary organic aerosol estimation, *Atmos. Environ.*, 40, 7546-7556,
638 doi:10.1016/j.atmosenv.2006.07.018, 2006.

639 Seinfeld, J. H. and Pandis, S. N.: *Atmospheric Chemistry and Physics: from air pollution to*
640 *climate change*, 2nd Edition, John Wiley and Sons, Inc., Hoboken, New Jersey, 2006.

641 Stockwell, W. R., and Calvert, J. G.: The mechanism of the HO-SO₂ reaction, *Atmos.*
642 *Environ.*, 17, 2231-2235, doi:10.1016/0004-6981(83)90220-2, 1983.

643 Sun, Y., Zhuang, G., Tang, A., Wang, Y., and An, Z.: Chemical characteristics of PM_{2.5} and
644 PM₁₀ in haze-fog episodes in Beijing, *Environ. Sci. Technol.*, 40, 3148-3155, 2006.

645 Sun, Y., Wang, Z., Fu, P., Jiang, Q., Yang, T., Li, J., and Ge, X.: The impact of relative
646 humidity on aerosol composition and evolution processes during wintertime in Beijing, China,
647 *Atmos. Environ.*, *77*, 927-934, 2013a.

648 Sun, Y., Jiang, Q., Wang, Z., Fu, P., Li, J., Yang, T., and Yin, Y.: Investigation of the Sources
649 and Evolution Processes of Severe Haze Pollution in Beijing in January 2013, *J. Geophys.*
650 *Res.*, *119*, 4380-4398, 2014.

651 Sun, Y. L., Wang, Z. F., Fu, P. Q., Yang, T., Jiang, Q., Dong, H. B., Li, J., and Jia, J. J.:
652 Aerosol composition, sources and processes during wintertime in Beijing, China, *Atmos.*
653 *Chem. Phys.*, *13*, 4577-4592, doi:10.5194/acp-13-4577-2013, 2013b.

654 Tang, G., Wang, Y., Li, X., Ji, D., Hsu, S., and Gao, X.: Spatial-temporal variations in surface
655 ozone in Northern China as observed during 2009-2010 and possible implications for future
656 air quality control strategies, *Atmos. Chem. Phys.*, *12*, 2757-2776,
657 doi:10.5194/acp-12-2757-2012, 2012.

658 Wang, K., Zhang, Y., Nenes, A., and Fountoukis, C.: Implementation of dust emission and
659 chemistry into the Community Multiscale Air Quality modeling system and initial application
660 to an Asian dust storm episode, *Atmos. Chem. Phys.*, *12*, 10209-10237, 2012.

661 Wang, L. T., Wei, Z., Yang, J., Zhang, Y., Zhang, F. F., Su, J., Meng, C. C., and Zhang, Q.:
662 The 2013 severe haze over southern Hebei, China: model evaluation, source apportionment,
663 and policy implications, *Atmos. Chem. Phys.*, *14*, 3151-3173, doi:10.5194/acp-14-3151-2014,
664 2014.

665 Wang, Y., Zhuang, G., Sun, Y., and An, Z.: The variation of characteristics and formation
666 mechanisms of aerosols in dust, haze, and clear days in Beijing, *Atmos. Environ.*, *40*,
667 6579-6591, 2006.

668 Wang, Y., Yao, L., Wang, L., Liu, Z., Ji, D., Tang, G., Zhang, J., Sun, Y., Hu, B., and Xin, J.:
669 Mechanism for the formation of the January 2013 heavy haze pollution episode over central
670 and eastern China, *Sci. China Earth Sci.*, *57*, 14-25, 2014.

671 Wang, Z., Li, J., Wang, Z., Yang, W., Tang, X., Ge, B., Yan, P., Zhu, L., Chen, X., and Chen,
672 H.: Modeling study of regional severe hazes over mid-eastern China in January 2013 and its
673 implications on pollution prevention and control, *Sci. China Earth Sci.*, *57*, 3-13, 2014.

674 Wendisch, M., Hellmuth, O., Ansmann, A., Heintzenberg, J., Engelmann, R., Althausen, D.,
675 Eichler, H., Mueller, D., Hu, M., and Zhang, Y.: Radiative and dynamic effects of absorbing
676 aerosol particles over the Pearl River Delta, China, *Atmos. Environ.*, 42, 6405-6416, 2008.

677 Xing, L., Fu, T. M., Cao, J. J., Lee, S. C., Wang, G. H., Ho, K. F., Cheng, M. C., You, C. F.,
678 and Wang, T. J.: Seasonal and spatial variability of the OM/OC mass ratios and high regional
679 correlation between oxalic acid and zinc in Chinese urban organic aerosols, *Atmos. Chem.*
680 *Phys.*, 13, 4307-4318, doi:10.5194/acp-13-4307-2013, 2013.

681 Xu, J., Ma, J. Z., Zhang, X. L., Xu, X. B., Xu, X. F., Lin, W. L., Wang, Y., Meng, W., and
682 Ma, Z. Q.: Measurements of ozone and its precursors in Beijing during summertime: impact
683 of urban plumes on ozone pollution in downwind rural areas, *Atmos. Chem. Phys.*, 11,
684 12241-12252, doi:10.5194/acp-11-12241-2011, 2011.

685 Yang, F., Tan, J., Zhao, Q., Du, Z., He, K., Ma, Y., Duan, F., and Chen, G.: Characteristics of
686 PM_{2.5} speciation in representative megacities and across China, *Atmos. Chem. Phys.*, 11,
687 5207-5219, doi:10.5194/acp-11-5207-2011, 2011.

688 Yang, K., Dickerson, R. R., Carn, S. A., Ge, C., and Wang, J.: First observations of SO₂ from
689 the satellite Suomi NPP OMPS: Widespread air pollution events over China, *Geophys. Res.*
690 *Lett.*, 40, 4957-4962, 2013.

691 Yao, X. H., Chan, C. K., Fang, M., Cadle, S., Chan, T., Mulawa, P., He, K. B., and Ye, B. M.:
692 The water-soluble ionic composition of PM_{2.5} in Shanghai and Beijing, China, *Atmos.*
693 *Environ.*, 36, 4223-4234, doi:10.1016/s1352-2310(02)00342-4, 2002.

694 York, D., Evensen, N. M., Martinez, M. L., and Delgado, J. D.: Unified equations for the
695 slope, intercept, and standard errors of the best straight line, *Am. J. Phys.*, 72, 367-375,
696 doi:10.1119/1.1632486, 2004.

697 Zhang, J. K., Sun, Y., Liu, Z. R., Ji, D. S., Hu, B., Liu, Q., and Wang, Y. S.: Characterization
698 of submicron aerosols during a month of serious pollution in Beijing, 2013, *Atmos. Chem.*
699 *Phys.*, 14, 2887-2903, doi:10.5194/acp-14-2887-2014, 2014.

700 Zhang, Q., Streets, D. G., Carmichael, G. R., He, K., Huo, H., Kannari, A., Klimont, Z., Park,
701 I., Reddy, S., and Fu, J.: Asian emissions in 2006 for the NASA INTEX-B mission, *Atmos.*
702 *Chem. Phys.*, 9, 5131-5153, 2009.

703 Zhao, P. S., Zhang, X. L., Xu, X. F., and Zhao, X. J.: Long-term visibility trends and
704 characteristics in the region of Beijing, Tianjin, and Hebei, China, *Atmos. Res.*, 101, 711-718,
705 doi:10.1016/j.atmosres.2011.04.019, 2011.

706 Zhao, X. J., Zhang, X. L., Xu, X. F., Xu, J., Meng, W., and Pu, W. W.: Seasonal and diurnal
707 variations of ambient PM_{2.5} concentration in urban and rural environments in Beijing, *Atmos.*
708 *Environ.*, 43, 2893-2900, doi:10.1016/j.atmosenv.2009.03.009, 2009.

709 Zhao, X. J., Zhao, P. S., Xu, J., Meng, W., Pu, W. W., Dong, F., He, D., and Shi, Q. F.:
710 Analysis of a winter regional haze event and its formation mechanism in the North China
711 Plain, *Atmos. Chem. Phys.*, 13, 5685-5696, doi:10.5194/acp-13-5685-2013, 2013.

712 Zheng, B., Zhang, Q., Zhang, Y., He, K. B., Wang, K., Zheng, G. J., Duan, F. K., Ma, Y. L.,
713 and Kimoto, T.: Heterogeneous chemistry: a mechanism missing in current models to explain
714 secondary inorganic aerosol formation during the January 2013 haze episode in North China,
715 *Atmos. Chem. Phys. Discuss.*, 14, 16731–16776, doi:10.5194/acpd-14-16731-2014, 2014.

716 Zheng, G., Cheng, Y., He, K., Duan, F., and Ma, Y.: A newly identified calculation
717 discrepancy of the Sunset semi-continuous carbon analyzer, *Atmos. Meas. Tech. Discuss.*, 7,
718 377–399, doi:10.5194/amtd-7-377-2014, 2014.

719 Zhou, J. M., Zhang, R. J., Cao, J. J., Chow, J. C., and Watson, J. G.: Carbonaceous and Ionic
720 Components of Atmospheric Fine Particles in Beijing and Their Impact on Atmospheric
721 Visibility, *Aerosol Air Qual. Res.*, 12, 492-502, doi:10.4209/aaqr.2011.11.0218, 2012.

Table 1. General information on severe haze episodes in January 2013

		Episode I			Episode II			Episode III			January		
		Ave.	min	max	Ave.	min	max	Ave.	min	Max	Ave.	min	max
Meteoro- logy Data	Temperature (°C)	-4.63	-11.10	1.40	-2.79	-8.30	2.80	-1.26	-6.60	5.00	-2.94	-12.50	5.00
	RH(%)	31.16	13.50	58.50	56.59	27.20	77.60	55.05	27.10	79.70	47.97	13.50	88.30
	WS(m/s)	2.10	0.90	4.40	2.08	1.00	3.40	1.96	0.90	3.60	2.18	0.90	4.50
PM_{2.5} and PM₁₀	PM _{2.5} (µg/m ³)	112.50	11.00	311.50	245.37	21.10	855.10	167.66	35.40	387.30	161.77	4.40	855.10
	PM ₁₀ (µg/m ³)	152.17	28.80	411.00	327.17	31.60	1157.50	214.03	41.50	479.80	223.53	13.90	1157.50
	PM _{2.5} /PM ₁₀ (%)	0.69			0.75			0.79			0.70		
Gas Data	NO ₂	76.39			109.44			95.86			86.09		
	SO ₂	79.73			123.35			63.86			77.54		

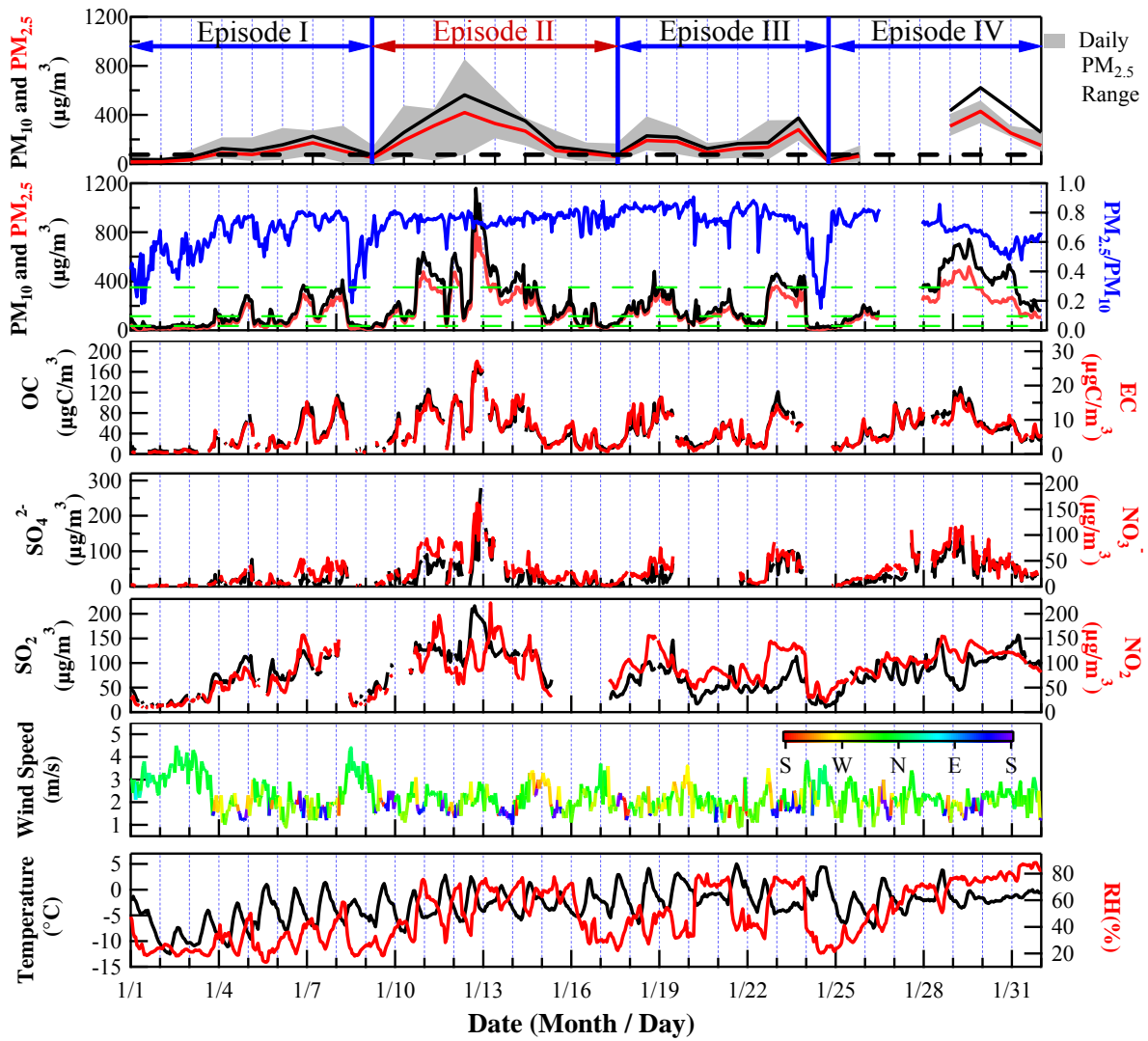


Figure 1. Time series of PM_{10} , $PM_{2.5}$, and its major components (OC , EC , SO_4^{2-} and NO_3^-), and meteorological data (wind speed, wind direction, temperature and relative humidity) for January 2013.

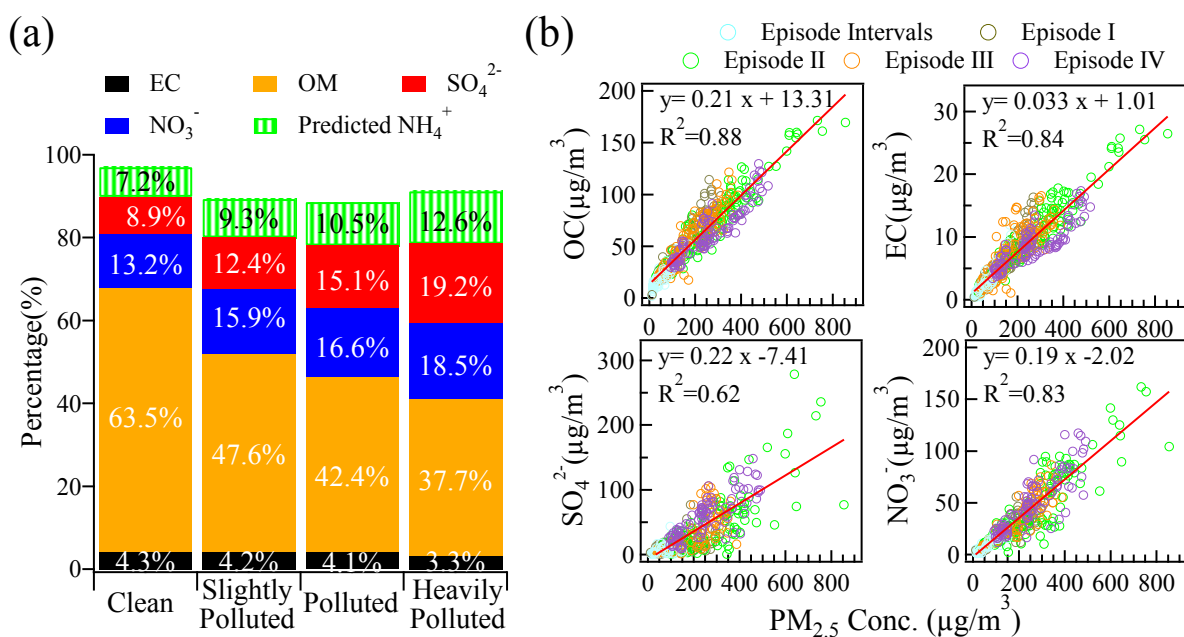


Figure 2. Major composition of PM_{2.5} with respect to pollution level. (a) Mean percentile composition and (b) hourly concentration of individual species plotted against PM_{2.5} mass concentration. Values showed in (a) were derived as average of ratios.

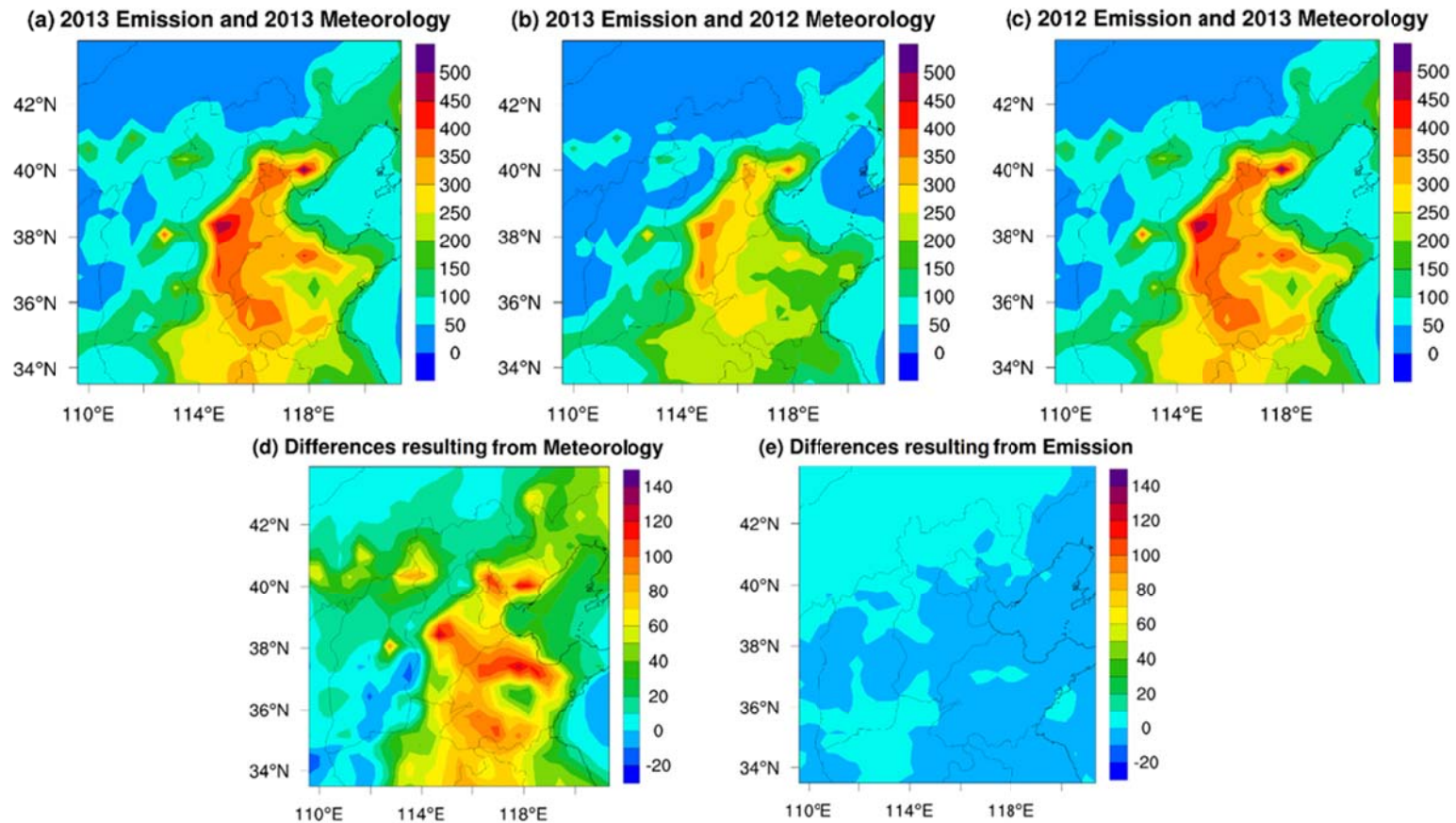


Figure 3. Revised WRF-CMAQ simulated monthly-averaged PM_{2.5} concentration (µg/m³) under different scenarios. (a) Base scenario. Actual Jan. 2013 emission and Jan. 2013 meteorology data were used. (b) Jan. 2012 meteorology data were used, and (c) Jan. 2012 emissions were used. The different PM_{2.5} concentrations (µg/m³) caused by meteorology (d; equivalent to a–b) and emission (e, equivalent to a–c) are also shown.

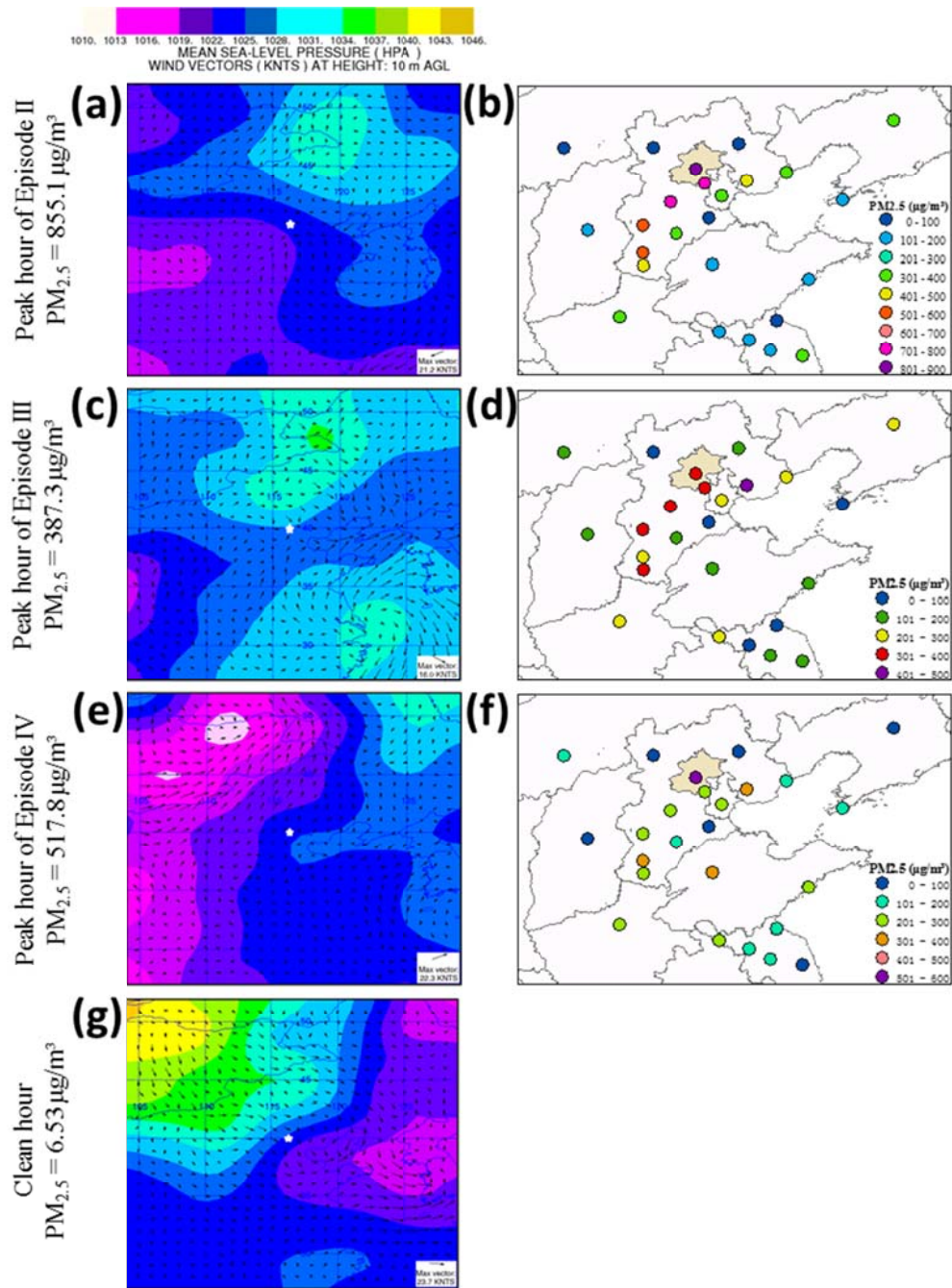


Figure 4. Surface weather maps (a, c, e, g) and $PM_{2.5}$ concentrations (b, d, f) of the North China Plain on 12 Jan. LT 18:00 (a, b), 18 Jan. LT 20:00 (c, d), 29 Jan. LT 13:00 (e, f), and 1 Jan. LT 8:00 (g). The location of Beijing is indicated as a white star on the weather maps, and as the shaded area on the $PM_{2.5}$ concentration maps. $PM_{2.5}$ concentrations in Beijing at the four selected time points are also shown on the left for reference.

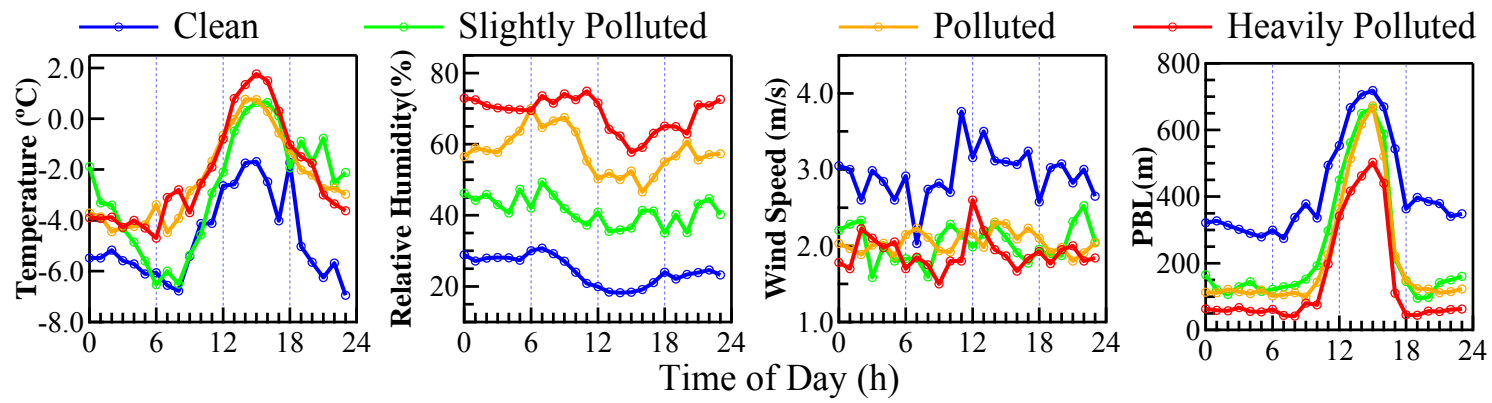


Figure 5. Mean diurnal variation in meteorological parameters for different pollution levels.

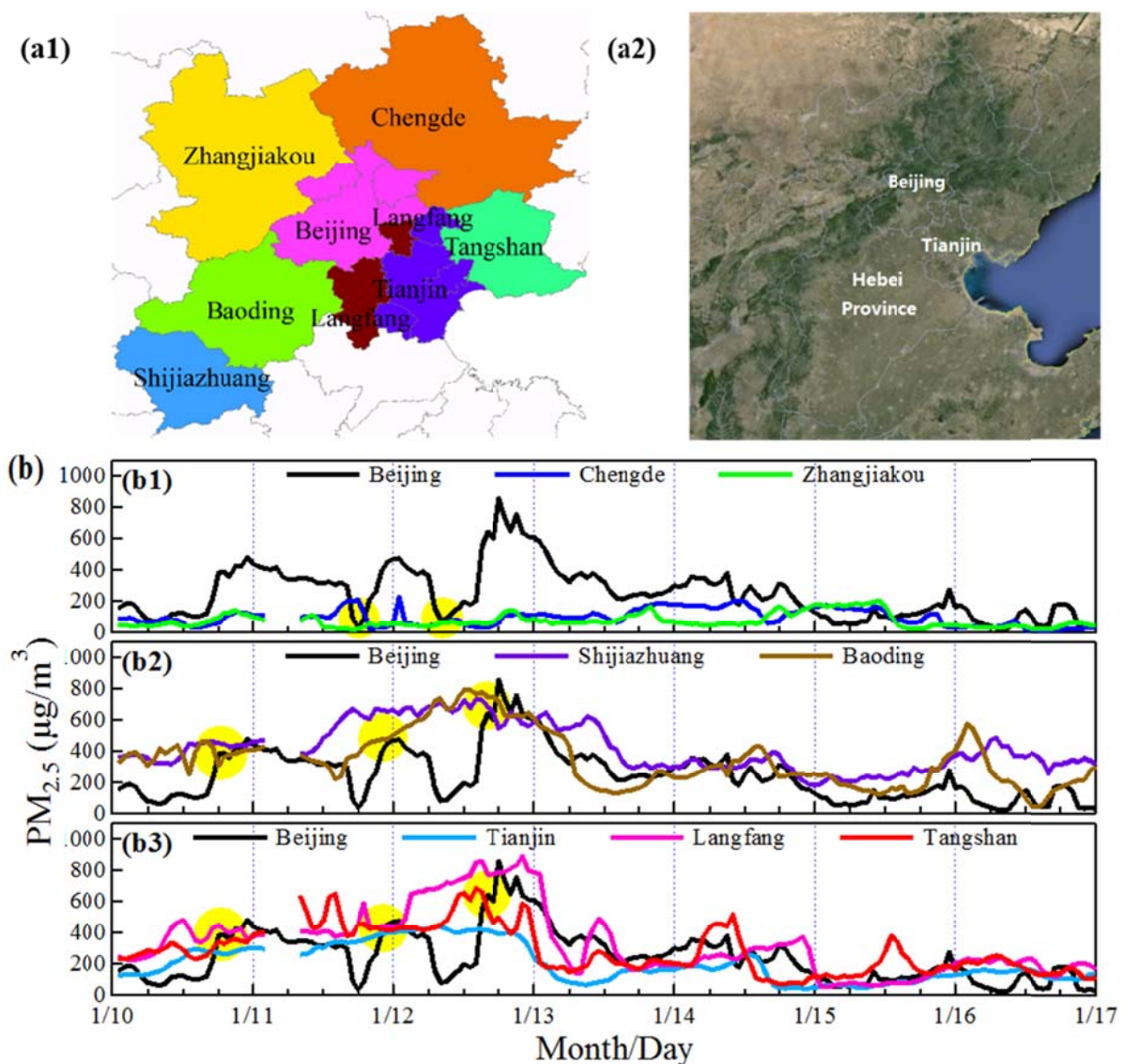


Figure 6. (a1) The location of all cities shown below, and (a2) topographic map around Beijing. (b) PM_{2.5} concentrations of Beijing and its (b1) northern cities, (b2) southwest cities, and (b3) southeast cities for the period 10–17 Jan. 2013. Yellow solid circles indicated the time periods when the sharp drops (b1) and sharp increases (b2 and b3) of PM_{2.5} concentration occurred.

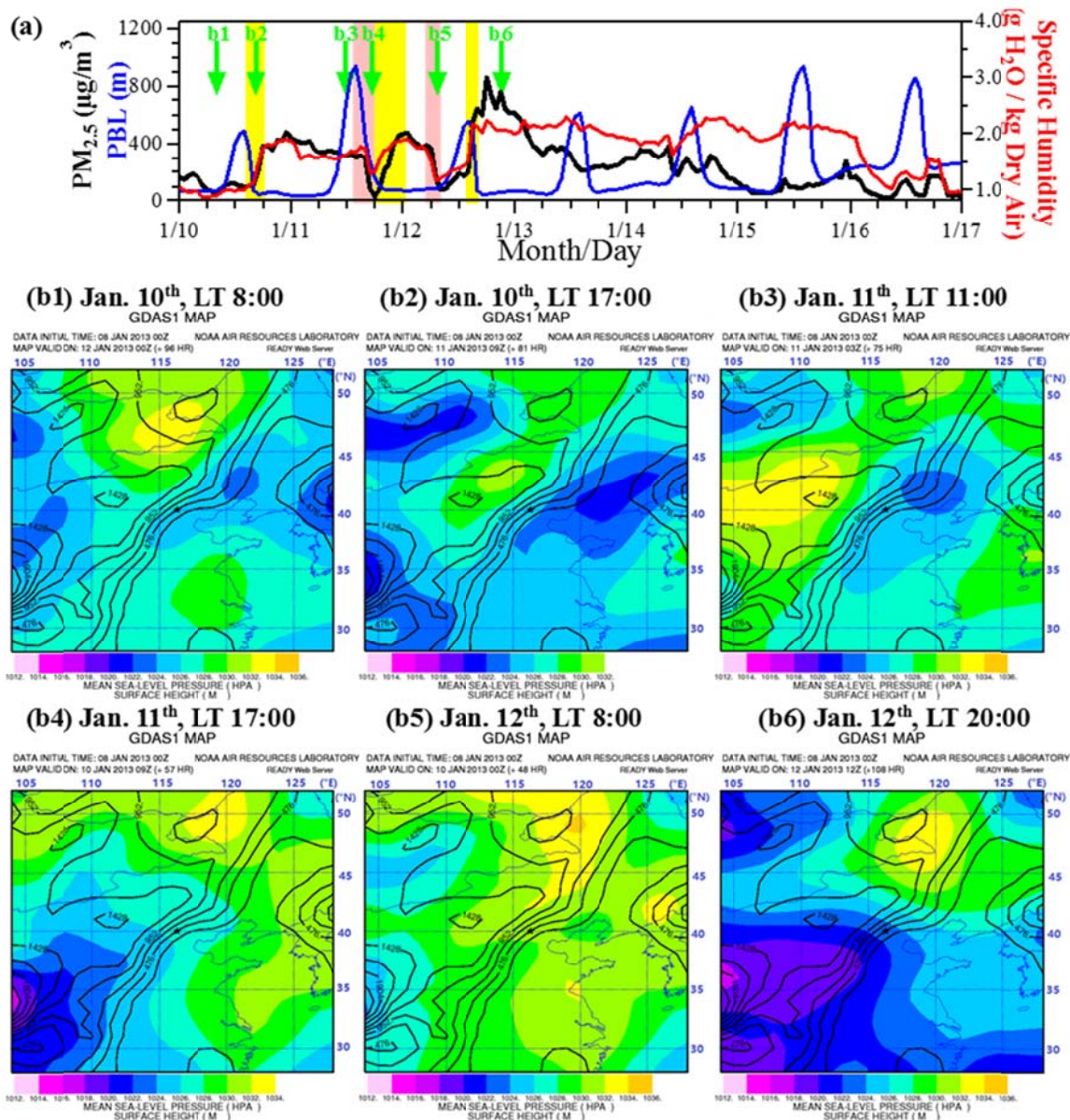


Figure 7. Evidence for regional transport of pollutants as a major factor contributing to sharp concentration increases in Beijing. (a) PM_{2.5} concentration, PBL height, and specific humidity in Beijing for 10–17 Jan. 2013. Pink and yellow rectangles indicated the sharp drop and sharp increase periods of PM_{2.5}, respectively. Note how nicely specific humidity and PM_{2.5} followed each other during these periods. (b) Weather patterns before and after the sharp increases events. Corresponding time point of b1 to b6 was indicated by arrows in (a). The topography map (elevation) is also shown for reference. Location of Beijing was indicated by the black star in center of each graph.

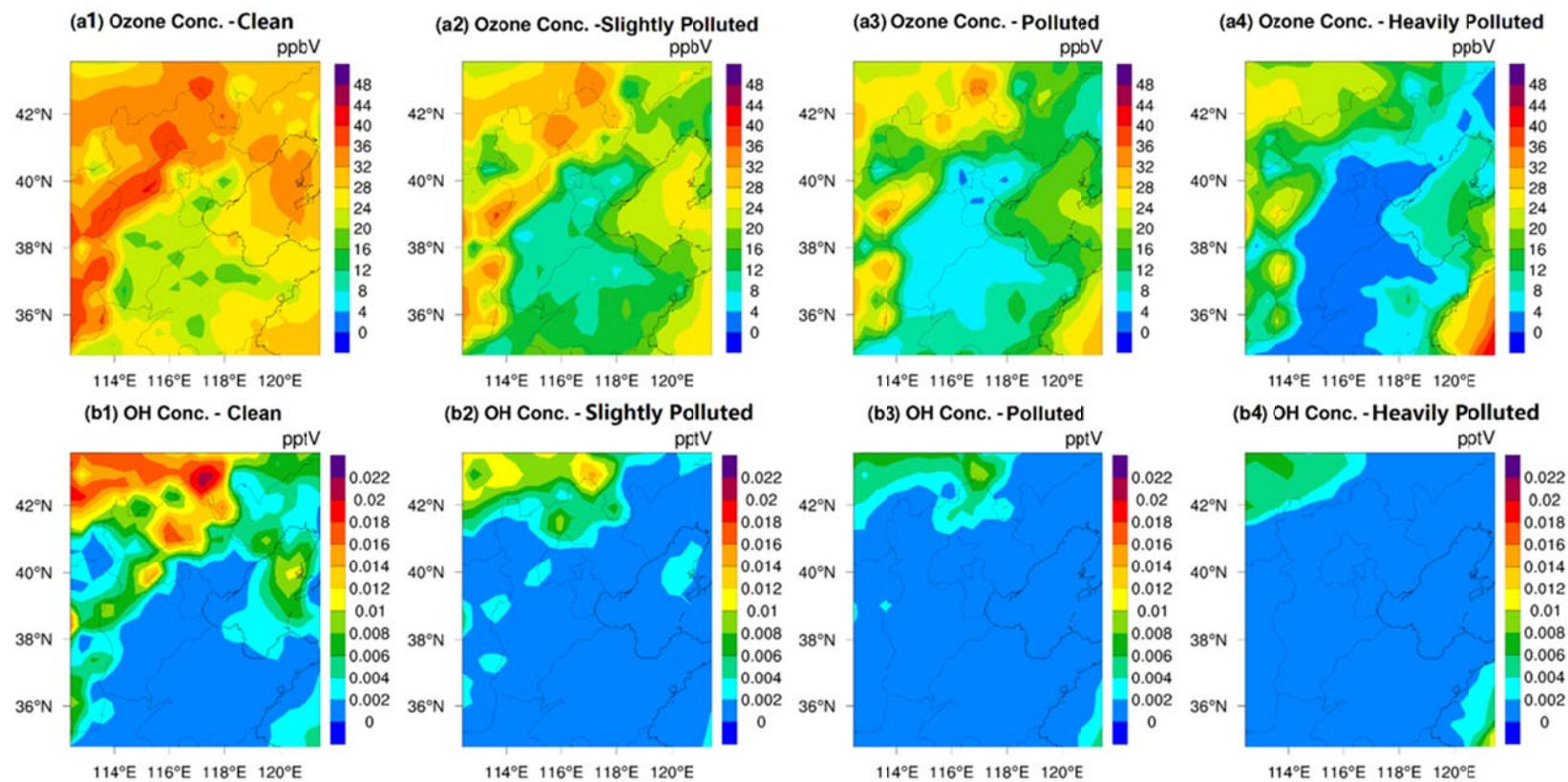


Figure 8. Revised WRF-CMAQ simulated regional distribution of daytime (7:00 ~ 18:00) concentration of (a) O₃ (ppbV) and (b) OH (pptV) at different pollution level.

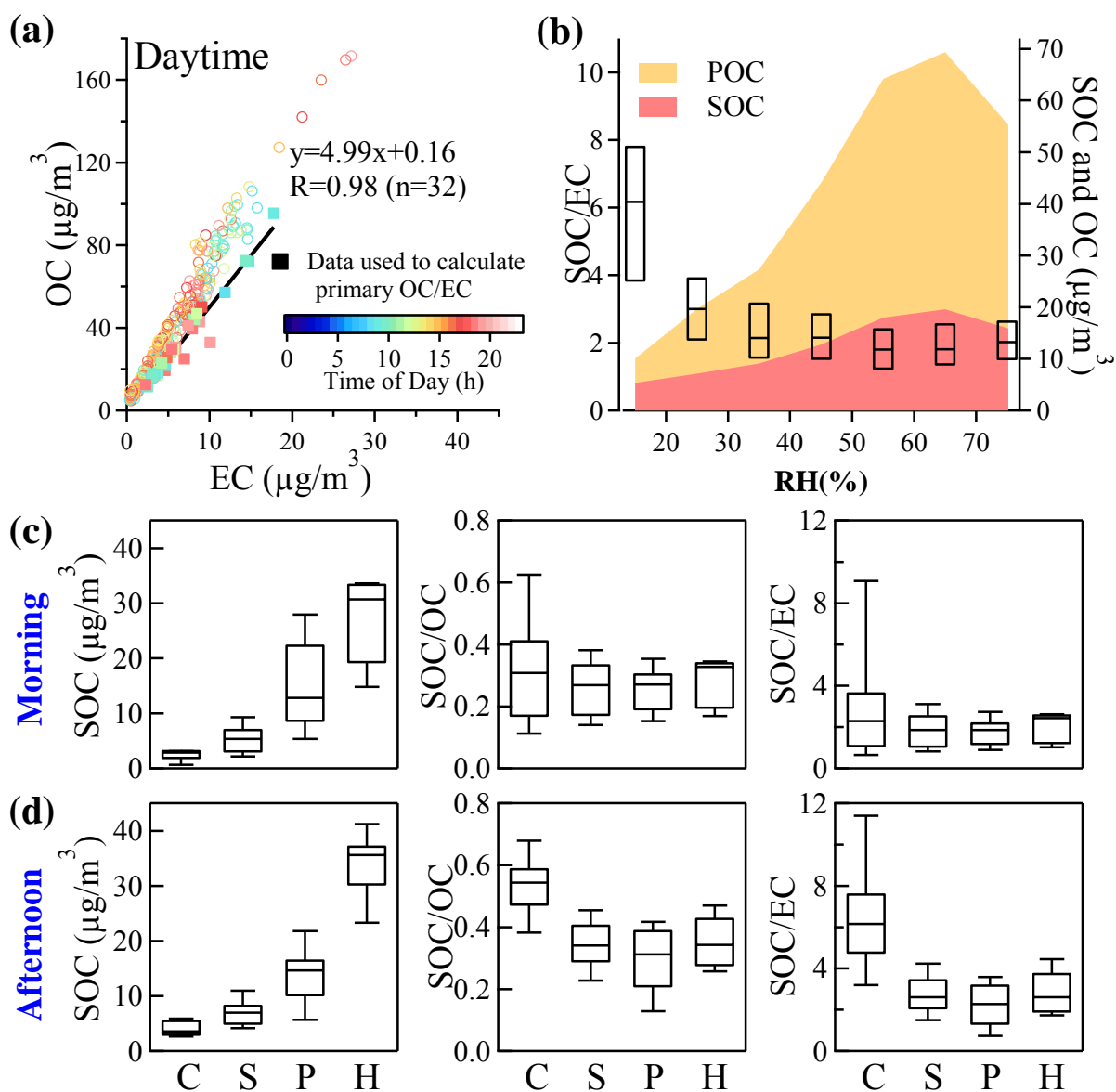


Figure 9. Evaluation of SOC formation. (a) Estimation of SOC with EC-tracer method. Squares indicate data used to calculate primary OC/EC, while open circles indicate other OC/EC data. (b) Change of SOC, OC and SOC/EC with RH. Data points shown in a and b referred to hourly concentrations in daytime (7:00~18:00). (c)-(d) Variation of SOC, SOC/OC and SOC/EC (c) in the morning (7:00~12:00) and (d) in the afternoon (13:00~18:00) with pollution level. “C”, “S”, “P”, “H” refer to “clean”, “slightly polluted”, “polluted” and “heavily polluted”, respectively. In the box-whisker plots, the boxes (b, c, d) and whiskers (c, d) indicated the 95th, 75th, 50th (median), 25th and 5th percentiles, respectively.

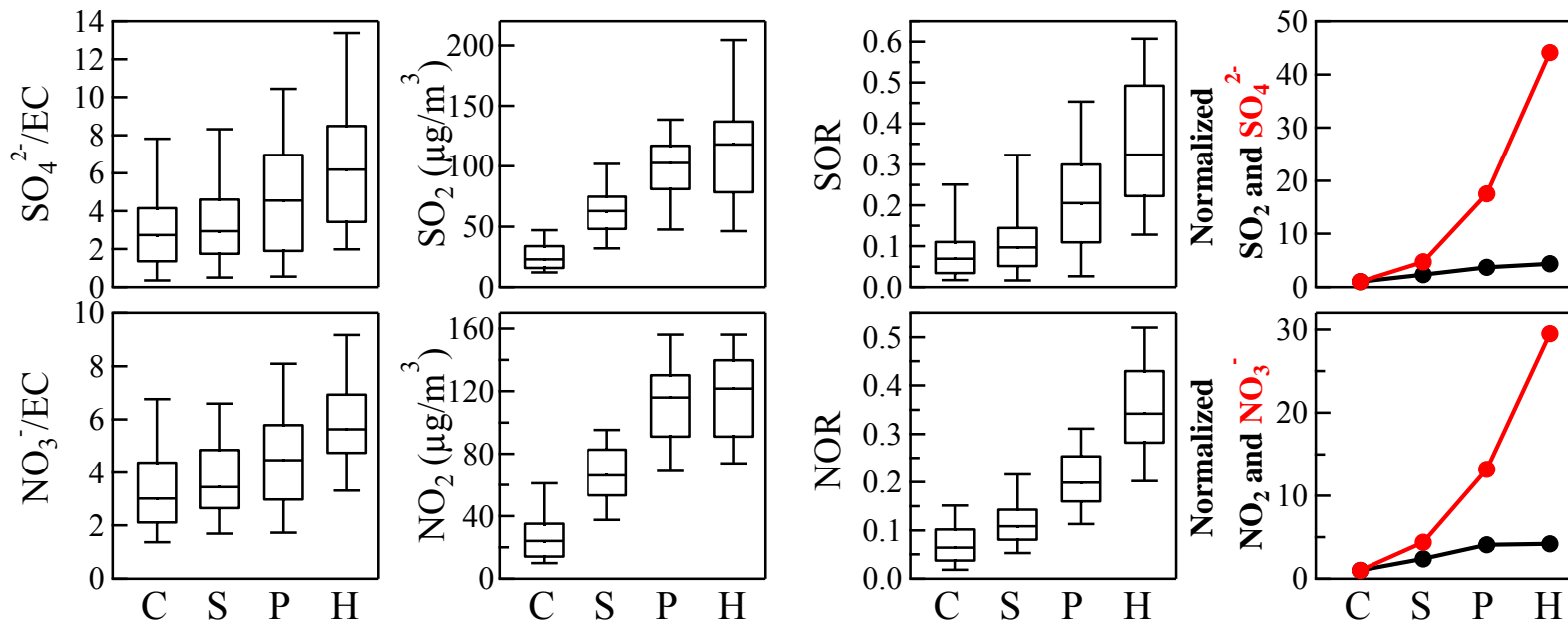


Figure 10. Variation of $\text{SO}_4^{2-}/\text{EC}$, NO_3^-/EC , SO_2 , NO_2 , SOR and NOR with pollution level. “C”, “S”, “P”, “H” refer to “clean”, “slightly polluted”, “polluted” and “heavily polluted”, respectively. Normalized X in Column 4 refers to the average concentration of X in any pollution level, scaled by its average concentration during clean periods. In the box-whisker plots, the boxes and whiskers indicated the 95th, 75th, 50th (median), 25th and 5th percentiles, respectively.

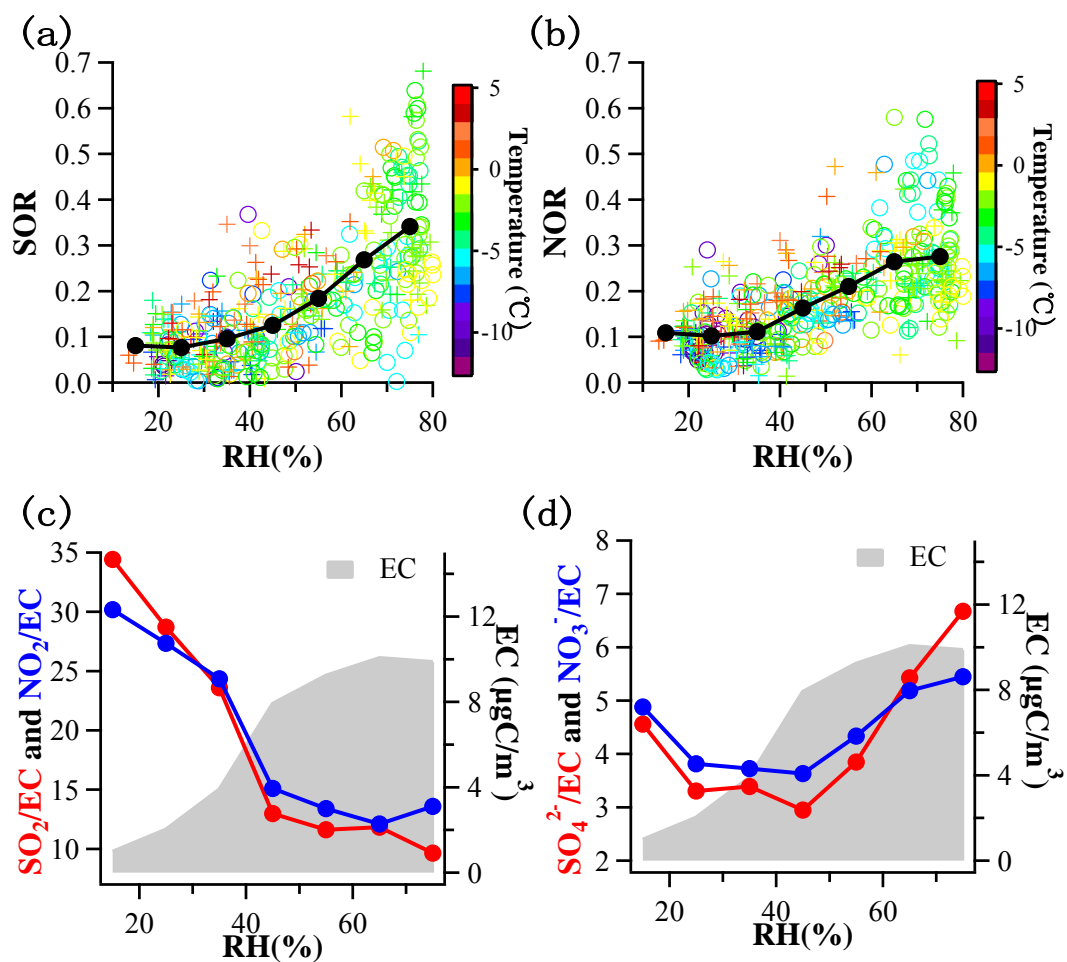


Figure 11. Importance of heterogeneous chemistry in sulfate and nitrate formation. (a-b) Hourly SOR and NOR plotted against RH, colored with temperature. (c-d) EC-scaled precursors (SO_2 and NO_2) and products (SO_4^{2-} and NO_3^-) plotted against RH. EC concentrations at different RH levels were shown for reference.

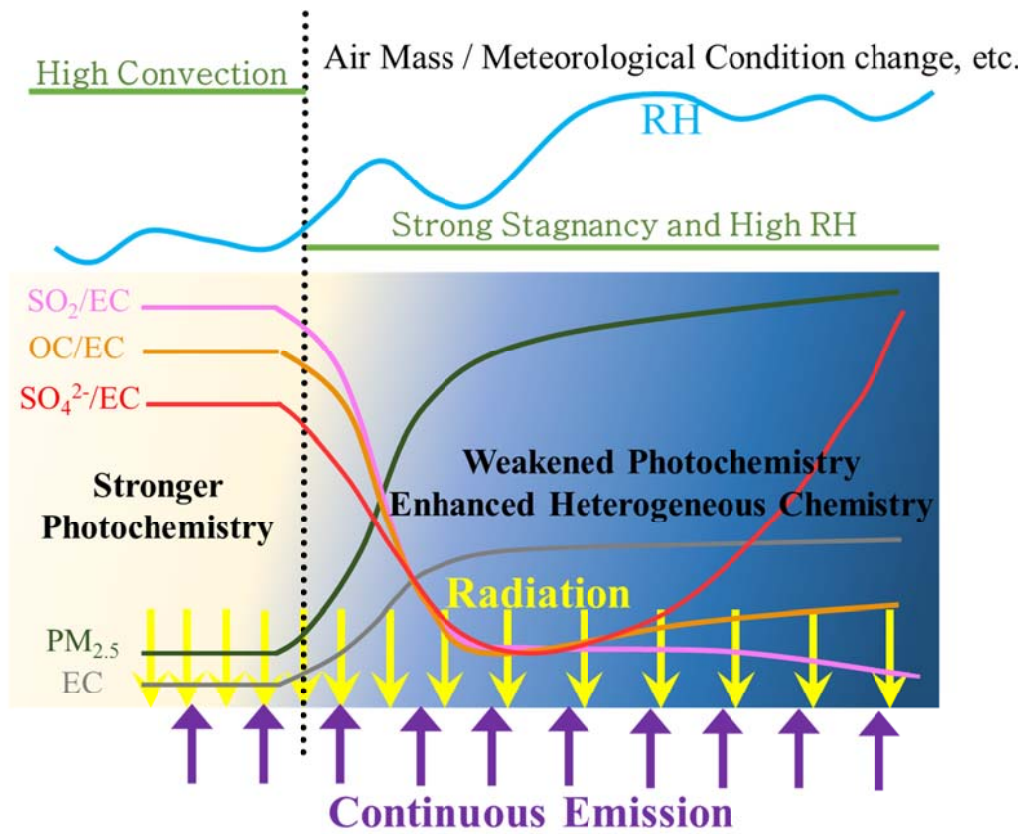


Figure 12. Conceptual model of atmospheric chemistry during the heavy pollutions. The dotted black line indicated the meteorology changed from convection-favoring condition to stagnant condition.